

Estimation of Forest Parameters Using 3D Satellite Data

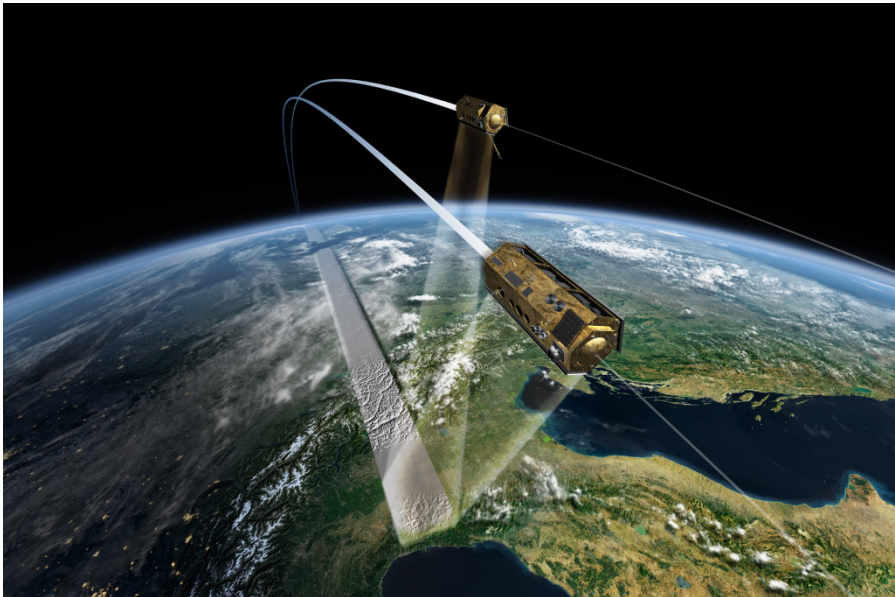
Stereogrammetry, radargrammetry and interferometry

Henrik Persson

Faculty of Forest Sciences

Department of Forest Resource Management

Umeå



Doctoral Thesis
Swedish University of Agricultural Sciences
Umeå 2014

Acta Universitatis agriculturae Sueciae

2014:84

Cover: Illustration of the double satellite formation, TerraSAR-X/TanDEM-X.
(DLR, German Aerospace Centre)

ISSN 1652-6880

ISBN (print version) 978-91-576-8116-4

ISBN (electronic version) 978-91-576-8117-1

© 2014 Henrik Persson, Umeå

Print: SLU Service/Repro, Uppsala/Alnarp 2014

Estimation of Forest Parameters Using 3D Satellite Data

Abstract

Accurate data about the forest are needed both in climate research and forest management planning. This thesis focuses on using different types of three-dimensional (3D) satellite data sources to accurately estimate forest variables, primarily above-ground biomass (AGB) and tree height (H). Different satellite sensors have been used and compared, and depending on the sensors, the acquired satellite images have been processed in different ways to create 3D surface models. The three main processing alternatives have been stereogrammetry, radargrammetry and interferometry. The surface models were used together with digital terrain models from airborne laser scanning, to take the difference between the two in order to create canopy height models. The models have been built and evaluated on data from two test sites: Krycklan located in northern Sweden (Lat. 64°N, Long. 19°E) and Remningstorp in southern Sweden (Lat. 58°N, Long. 13°E).

The included studies have shown that 3D satellite data are efficient to use for accurate estimations of AGB and H at stand-level. Moreover, the optical stereogrammetric models can play a role in the boreal region, but to obtain accurate estimations they are dependent on rather high resolution, along-track data with pixel sizes smaller than 10 m. Radargrammetry applies stereogrammetry to radar images, which can be taken regardless of atmospheric conditions, time of day, or season. Data from TerraSAR-X were used and AGB and H could be estimated with 22.9% and 7.7% root mean square error (RMSE), respectively, at stand-level. Interferometry was applied to data from the TanDEM-X mission and this technique was superior to stereogrammetric and radargrammetric techniques, where AGB and H could be estimated with 14.4% and 4.1% RMSE, respectively, at stand-level.

The first three studies in this thesis used empirical approaches and in contrast to this, the last two studies employed the two-level model (TLM), which has been developed with semi-empirical modeling based on simplified physical reasoning. The TLM also used TanDEM-X data and this showed potential for even more accurate predictions of forest related variables.

To conclude, this thesis shows the potential of 3D satellite data as a highly reliable and a widely applicable remote sensing data source for estimation of forest parameters.

Keywords: forest, biomass, tree height, forest density, satellite, optical, radar, SAR, stereogrammetry, radargrammetry, interferometry, TanDEM-X, ALOS-PRISM

Author's address: Henrik Persson, SLU, Department of Forest Resource Management, Skogsmarksgränd, SE-901 83 Umeå, Sweden. *E-mail:* Henrik.Persson@slu.se

"Un bon croquis vaut mieux qu'un long discours"
(A picture is worth a thousand words)

Napoleon Bonaparte

Contents

List of publications	7
Abbreviations	9
1 Introduction	11
1.1 Forests	13
1.1.1 Forest variables	13
1.1.2 Field reference data	15
1.2 Optical imagery and stereogrammetry	15
1.3 Radar basics	18
1.3.1 Basic principles	18
1.3.2 Resolution of real-aperture radar	21
1.3.3 Complex electromagnetic signals	23
1.3.4 Radar scattering	26
1.3.5 Geometric effects	27
1.4 Synthetic aperture radar	28
1.4.1 Spatial resolution	30
1.4.2 Image characteristics	31
1.5 Radargrammetry	32
1.6 Interferometry	37
1.6.1 Interferometric phase	37
1.6.2 Height of ambiguity	40
1.6.3 Interferometric coherence	41
1.6.4 Theoretical relationships between InSAR and forest parameters	41
1.6.5 Interferometric Water Cloud Model	42
1.6.6 Random Volume over Ground	44
1.6.7 Forest research based on InSAR	47
1.7 Concluding remarks	50
2 Objectives	53
3 Material and methods	55
3.1 Materials	55
3.1.1 Test sites	55
3.1.2 Reference data	55
3.1.3 Satellite data	58
3.1.4 Other data sources	58

3.1.5	Paper I - Stereogrammetry	58
3.1.6	Papers II-V - Radargrammetry or interferometry	60
3.2	Analysis methods	60
3.2.1	Data processing	60
3.2.2	Paper I - Stereogrammetry	61
3.2.3	Paper II - Radargrammetry	62
3.2.4	Paper III - Interferometry	62
3.2.5	Paper IV – Two-level model inversion of tree height and canopy density	63
3.2.6	Paper V – Two-level model based inversion of AGB	65
3.2.7	Model analysis	65
3.2.8	Accuracy assessment	66
4	Results and discussion	69
4.1	Stereogrammetry	71
4.2	Radargrammetry	72
4.3	Interferometry	74
4.4	Concluding remarks	76
4.5	Future work	77
	References	79
	Acknowledgments	93

List of publications

This thesis is based on the work contained in the following papers, referred to by Roman numerals in the text:

- I Persson, H., Wallerman, J., Olsson, H. and Fransson, J. E. S. (2013). Estimating forest biomass and height using optical stereo satellite data and a DTM from laser scanning data. *Canadian Journal of Remote Sensing* 39(3), 251-262.
- II Persson, H. and Fransson, J. E. S. (2014). Forest variable estimation using radargrammetric processing of TerraSAR-X images in boreal forests. *Remote Sensing* 6(3), 2084-2107.
- III Persson, H. and Fransson, J. E. S. Comparison between TanDEM-X and ALS based estimation of biomass and tree height in boreal forests (submitted manuscript).
- IV Soja, M. J., Persson, H. and Ulander, L. M. H. Estimation of forest height and canopy density from a single InSAR correlation coefficient (in press for publication in *IEEE Geoscience and Remote Sensing Letters*).
- V Soja, M. J., Persson, H. and Ulander, L. M. H. Estimation of forest biomass from two-level model inversion of single-pass InSAR data (submitted manuscript).

Papers I, II and IV are reproduced with the permission of the publishers.

The contribution by Henrik Persson to the papers included in this thesis was as follows:

- I Planned the study with the co-authors. Carried out all data processing and wrote the major part of the manuscript.
- II Planned the study with the main supervisor. Carried out all data processing and wrote the major part of the manuscript.
- III Planned the study with the main supervisor. Carried out all data processing and wrote the major part of the manuscript.
- IV Involved in the discussions about the model, contributed with the field data and some analyses of these and described the temporal forest management activities during the investigated time period. Wrote a minor part of the manuscript.
- V Involved in the discussions about the model. Carried out field data analysis, error estimations and predictions of reference data. Wrote a minor part of the manuscript.

Abbreviations

3D	Three-Dimensional
AGB	Above-Ground Biomass
ALOS	Advanced Land Observing Satellite
ALS	Airborne Laser Scanning
ASTER	Advanced Spaceborne Thermal Emission and Reflection Radiometer
CHM	Canopy Height Model
DBH	Diameter at Breast Height
DEM	Digital Elevation Model (height model which can be of the ground or both ground and objects)
DLR	German Aerospace Center
DTM	Digital Terrain Model (height model of the ground)
EM	Electromagnetic
GCP	Ground Control Point
HOA	Height Of Ambiguity
InSAR	Interferometric SAR
IWCM	Interferometric Water Cloud Model
m.a.s.l.	Meters Above Sea-Level
NFI	National Forest Inventory
PRF	Pulse Repetition Frequency
PRISM	Panchromatic Remote-sensing Instrument for Stereo Mapping
RAR	Real-Aperture Radar
REDD	Reducing Emissions from Deforestation and forest Degradation
RMSE	Root Mean Square Error
RVoG	Random Volume over Ground
SAR	Synthetic Aperture Radar

SLU	Sveriges Lantbruksuniversitet (Swedish University of Agricultural Sciences)
SPC	Scattering Phase Center
SPOT	Satellite Pour l'Observation de la Terre (Satellite for observation of Earth)
TanDEM-X	TerraSAR-X add-on for Digital Elevation Measurement
TDX	TanDEM-X (the single satellite and not the mission)
TLM	Two-Level Model
TSX	TerraSAR-X
VR	Vegetation Ratio



1 Introduction

Global warming caused by human activities is one of the most important environmental challenges facing the world today. Global warming is leading to climate changes that will strongly influence the lifestyle of human beings around the globe, have impacts on food production systems, and lead to a rise of the global ocean level, among other effects. Emission of greenhouse gases, including carbon dioxide, is a main reason for this and by improving our understanding of the global carbon cycle, a faster and smarter adaptation and mitigation to the changing climate can be achieved (Stocker et al. 2013).

A vital part of understanding the global carbon cycle comprises carbon flux and therefore also emissions and sequestration of carbon. The main feature in the contemporary CO₂ records is the long-term increase of CO₂ in the terrestrial biosphere, that over time has acted as a carbon sink (Canadell et al. 2007). Land vegetation comprises 2477 Gt biomass (the mass of living organic matter) and the forests hold about 466 Gt (19%) of the planet's terrestrial carbon (Watson et al. 2000), the rest is stored in the soil. It is difficult and complex to efficiently measure the distribution of forest biomass and biomass change globally (Pan et al. 2011). Despite the forests' limited share in the global carbon flux, it has been shown to have important short- and long-term sequestration potential (Wardle et al. 2003; Cornwell et al. 2008; Brovkin et al. 2012; Makkonen et al. 2012) and the impact of forest activities has explicitly been mentioned in the Kyoto protocol (United Nations 1998).

As one part of improving this knowledge, the United Nations Programme on Reducing Emissions from Deforestation and Forest Degradation in Developing Countries (UN-REDD Programme) has been initiated, which also supports nationally-led REDD+ processes. It brings together technical teams from around the world to develop common

approaches, analyses and guidelines on issues such as measurement, reporting and verification (MRV) of carbon emissions and flows, greenhouse gasses, and inventories based on remote sensing.

Swedish forests have in the past been extensively used for timber production which has largely altered them (Lämås 1996). Therefore many plants and animals have become rare and are sometimes placed also on red-lists. Contemporary forest management planning aims for both timber production and to maintain biodiversity, where both are of equal importance. This includes strategic, tactical and operational planning. The strategies balance the different aims of optimized timber production and maintained biodiversity, both locally and at company level. The tactical planning turns the strategies into applied forestry, concerning allocation and degree of forest operations at different times. Operational planning concerns the forest treatments, such as felling and scarification. Many influencing parameters have to be considered and for this purpose, decision support systems, for example, the Heureka system as described in Wikström et al. (2011), have been developed. Traditionally, inventories have been used as a data input to systems for decisions at different levels and different time horizons. For efficiency and precision, both time- and cost-wise, remote sensing data can play an important role in such systems.

The term “remote sensing”, introduced in the 1960s, describes the acquisition of information about an object or phenomenon without making physical contact with the object and is thus in contrast to *in situ* observation. Throughout this thesis, flying platforms consisting of airplanes or satellites are used as the observation platform if nothing else is explicitly stated.

By using airborne laser scanning (ALS) data, precise information about the forest structure can be collected and by relating these to known (measured) tree height or estimated biomass at reference plots in the region scanned, accurate estimations of the current state of the forest can be obtained (Hyypä et al. 2008). ALS has been considered the most accurate remote sensing technique currently available (Nilsson 1996; Næsset 1997b; Næsset 1997a; Næsset 2002; Reutebuch et al. 2003; Næsset et al. 2004; St-Onge et al. 2008). It relies on use of airplanes or helicopters as the airborne platform and has become widely used for many countries’ national land surveys in order to establish accurate digital terrain models (DTMs), e.g. Denmark, Norway, Finland, Spain, Poland, England and Wales, the Netherlands and Switzerland. These ALS data can potentially also be used for estimations of the national forest states. The establishment in the case of Sweden is currently taking place and has been estimated to about 6 years

(Bergström et al. 2009). Despite the highly accurate forest state data ALS can provide, it seems it cannot take on the full task of being the only solution for providing high-frequency acquisitions of the entire globe.

Satellite-borne sensors can cover large areas and often have very short repeat periods, commonly within one to two weeks. When a DTM is present, which describes the elevation of the bare ground, satellite sensors can provide the frequent inventory data needed to predict forest variables such as tree height or biomass. In specific, tree height can be retrieved from a canopy height model (CHM) obtained by taking the difference between the forest top elevation, also denoted digital surface model (DSM), and the DTM. Luckily the ground elevation remains rather constant over time (at least compared to the vegetation) and the ALS data (which are collected in most developed countries) can also be used to generate accurate DTMs as a complement to providing accurate information about the forest state. Therefore all components are available in order to construct efficient forest biomass estimation tools.

1.1 Forests

Sweden consists of 40.8 million ha land and out of these 28.1 million ha are forest land of which 23.1 million ha (57%) are productive forest land (Swedish National Forest Inventory 2013). The unproductive forest includes, for example, mires and mountain forest (where the forest does not grow enough to be counted as productive forest land). About 95% of the productive forest has been felled the last 150 years. Sweden is mainly composed of boreal forest which makes up about 1/3 of the global total forest area but only ~19% of the global carbon stock. The boreal forest zone covers large parts of Scandinavia, Finland, northern Russia, Canada and Alaska (Watson et al. 2000). The forest remote sensing research carried out in this thesis is hence applicable to large parts of the world and with some modifications, often transferable to most of the world's forests. In Sweden, the stem volume distribution is mainly distributed on Scots pine (*Pinus Sylvestris* L.) (39.3%) and Norway spruce (*Picea abies* (L.) Karst.) (41.3%), while birch (*Betula* spp.) is by far the most abundant deciduous tree species (12.4%) (Swedish National Forest Inventory 2013).

1.1.1 Forest variables

Accurate climate models require accurate input data (World Meteorological Organization 2014), with remote sensing as a potential data source. Remote sensing in Sweden has nevertheless long also been intimately integrated

with the forest industry (and private forest owner associations). These forestry interest groups care about directed forest management, and to have a strong decision basis many different forest variables might be of interest, depending on their respective requirements.

Obvious measures that can be undertaken manually in a forest are stem diameter (defined as diameter at breast height, DBH, 1.3 m above ground), tree height and species. Other variables that are more complicated to measure directly are, for example, stem volume, biomass and forest density. Therefore detailed studies have been published, including formulas that relate the directly available measurable variables to the indirect ones. For the purpose of estimating stem volume, biomass and tree growth predictions in Sweden, the most cited papers are by Näslund (1947), Marklund (1987; 1988), and Söderberg (1986) in which detailed formulas are presented regarding how to calculate for example branch biomass when the stem diameter and species are known. Common terms are stem volume (over bark measured from stump to top of bole) and above-ground biomass (AGB), defined as all biomass above the soil including stem, branches, bark, and needles, excluding stumps, roots, foliage and flowers. The AGB is frequently used in climate related discussions while the former is typically used by the industry. The biomass is related to stem volume with a scaling factor being the wood density for that species, and typically has a value between 0.5-0.7 g/cm³.

Concurrently remote sensing is breaking ground quickly and historic measures like DBH might no longer be the most convenient input variable to be used to calculate indirect variables. New techniques such as calibrated ALS data have increasingly become considered superior compared to manual field measures, especially for tree height.

The variables mentioned so far have all been related to single trees but where a forest is concerned, other metrics like height variance, species composition and number of trunks can also be of interest. In forest remote sensing, the term H_{100} is frequently used to describe the arithmetic mean height of the 100 tallest trees ha⁻¹. By using a relascope, the basal area can be derived simply. In Sweden (and throughout this thesis) the basal area-weighted mean height (also called Lorey's mean height), H , is preferred over H_{100} , which means that larger trees are weighted more in the calculations of the stand mean height. The basal area (BA) is simply the tree cross-section, $BA = \pi(DBH/2)^2$ [m²], at breast height. The term H_{100} can sometimes be used to describe the 100th height percentile in a raster cell, but in this thesis, the prefix p will be used (e.g., $p99$ for percentile 99).

1.1.2 Field reference data

The managed forest is divided into forest stands (typically ~0.5-10 ha large), where each stand consists of roughly homogenous forest, often with mainly the same species and age class. This classification can be natural (because of changing land conditions such as rocks, mires, forest fires or storm damage) or achieved on purpose (e.g., that by some reason an entire stand is not suitable to completely clear-cut and new forest boundaries arise). One common way of collecting standwise field data for remote sensing studies has been to sample stands at a test site, where samples are taken at systematic locations within a stand and these are then assumed to represent the properties of the entire stand, under the pre-condition that the forest is roughly homogenous. By taking more samples or possibly changing the sampling design, the estimation accuracy might be increased.

Typically circular plots are used for sampling and these can be of varying size, often ~7-20 m radius. To do independent estimations of the state of Swedish forests, the Swedish National Forest Inventory (NFI) carries out inventories on about 11,000 field plots annually (Swedish National Forest Inventory 2013). These are distributed systematically and consist of temporary (visited only once) and permanent (revisited every fifth year) plots, where the temporary plots have 7 m radius and the permanent plots have 10 m radius.

Stem diameter and species are usually determined on all trees within a plot while a subset (e.g. by probability proportional to size, Ducey 2009) is used for a more exhaustive examination where, e.g., tree age, tree height or dead wood can be measured.

Field measures are expensive and time-consuming and this is where remote sensing plays an important role of bringing increased knowledge about the forest state with fewer manual field visits.

1.2 Optical imagery and stereogrammetry

Optical satellite data have been used for large-area biomass studies for years (Landsat 1 was launched 1972) and historically they have normally been recorded as 2D images. Different sensors can acquire data from different wavelengths, but common spectral bands include the wavelengths within the visible spectrum (~400-700 nm) and the near infrared band. Vegetation is commonly perceived as green, because wavelengths within the green region of the spectrum are reflected by pigments in the leaf, while other visible wavelengths are absorbed and used in the photosynthesis. The components in vegetation reflect, transmit and absorb different portions of

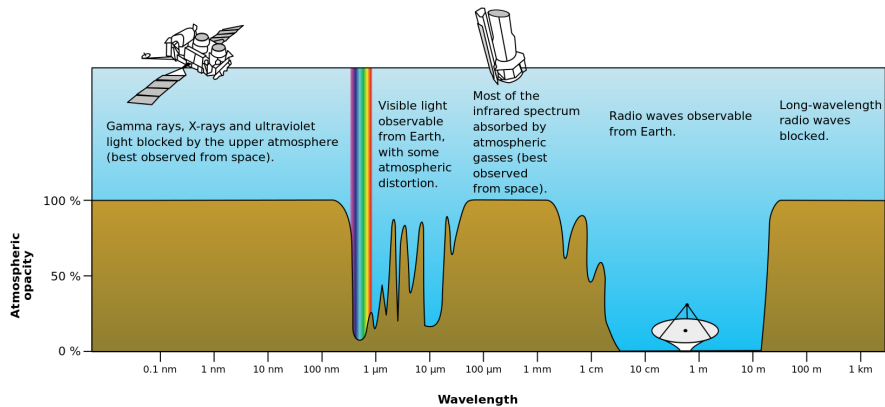


Figure 1. An illustration of the atmospheric opacity, with the “atmospheric windows” having close to 100% transparency.

the near-infrared radiation. Additionally, common bands cover the wavelengths within the “atmospheric windows”, which are wavelengths that pass less hindered through the atmosphere (Figure 1). Optical imagery relies on the sun as the only source of radiation and by analyzing the reflectance in all these bands, conclusions about, for example, vegetation types, health or biomass can be drawn.

In younger stages of a forest the electromagnetic (EM) radiation can reach different levels in the sparse canopy, which can be detected by optical sensors. At a certain development stage of the forest, the canopy tends to close while the stems can continue to grow and develop. Since the wavelengths used by an optical sensor do not penetrate the closed canopy, and therefore cannot collect the information necessary to assess biomass, the relationship between spectral 2D data and forest biomass tends to be poor for higher volumes with closed canopies (Knyazikhin et al. 1998; Myneni et al. 2002). This is often referred to as saturation of the signal. One solution to this has been to measure tree height metrics instead of reflected radiance by applying photogrammetric techniques - long known from the field of airborne remote sensing - to satellite images. The method is based on stereogrammetry, where two overlapping 2D images are acquired from slightly different look angles (due to change in view location) depicting the objects with minor differences (disparities). The further away from the sensor, the smaller the displacements will appear. These differences in displacements are used by our brains to sense vertical exaggeration and can be used by computers to determine object heights. In practice, this is computed for every pixel in a stereo pair and with larger disparities, height determination becomes stronger. On the other hand, the

ability to automatically find corresponding points in stereo pairs becomes more difficult.

Satellite sensors with a side-looking capability, providing appropriate optical images, have been available since the launch of SPOT-1 in 1986, however, acquiring cloud-free images is a common problem; getting two cloud-free images within two following orbits is uncommon. Along-track stereo imaging reduces these problems by having (at least) two sensors mounted on the same satellite platform, but directed in different directions along-track, usually forward and backward. Through this setup, the same projected region on the ground will first be covered slightly in front of the satellite and shortly thereafter from the backward looking sensor (depending on the look angle). The SPOT-5 satellite sensor has $\pm 20^\circ$ look angles and the time difference corresponds to 90 s (*Figure 2*).

Along-track stereo was first used in the 1960s when the United States operated the CORONA program of spy satellites that used photographic film. The German Aerospace Center (DLR) proved the feasibility of digital along-track stereo using push broom sensors in 1996 when the Modular Optoelectronic Multispectral Scanner (MOMS) sensor was operated from the MIR space station (Lehner & Müller 2003).

Stereo matching of data from the same acquisition occasion has the advantage of reducing radiometric image variations as well as reducing differences in cloud and atmospheric conditions, thereby improving the quality of the DSM in the image matching process (Toutin 2000). Further examples of sensors with along-track stereo imaging capability suitable for operational large-area mapping are SPOT-5 HRS (High Resolution Stereoscapy), Cartosat-1, Terra ASTER (Advanced Spaceborne Thermal Emission and Reflection Radiometer) and ALOS (Advanced Land Observing Satellite) PRISM (Panchromatic Remote-sensing Instrument for Stereo Mapping).

Few studies (to the authors' knowledge) using satellite stereogrammetry for AGB and H estimations have so far been carried out before the one presented in this thesis (Paper I). Büyüksalih & Jacobsen (2007) investigated the quality of DEM generation from the optical satellites IKONOS, QuickBird and OrbView-3 (all sensors with very high spatial resolution and data available for only limited parts of the world). Only stable regions in urban environments were examined and they found vertical accuracies between 1.7 m and 4.0 m. They also concluded that automatic image matching was more difficult with high-resolution images than with lower resolution.

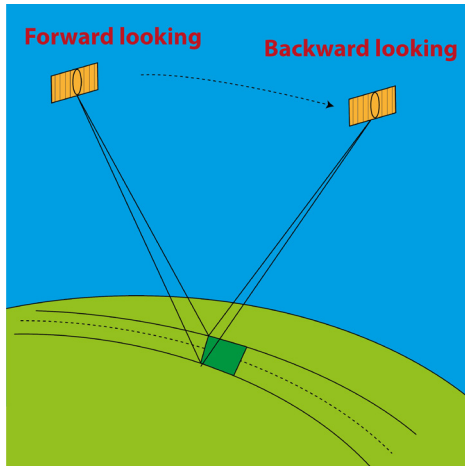


Figure 2. Illustration of along-track stereo imagery, where two sensors on the same satellite are covering the same ground region with a temporal difference.

One study that used SPOT-5 HRG (High Resolution Geometry) data in combination with stereogrammetry of airborne Z/I DMC data as well as SPOT-5 HRS data, was presented in Wallerman et al. (2010). The DTM was acquired from ALS. It was found that the H, stem diameter, and stem volume could be estimated with 7.3%, 9.0%, and 19% root mean square error (RMSE), respectively, when using SPOT-5 HRG and Z/I DMC data in combination. The SPOT-5 HRS CHM in combination with SPOT-5 HRG data improved the SPOT HRG based estimates from 13% to 10%, 15% to 13%, and 31% to 23% RMSE, for H, stem diameter, and stem volume, respectively.

1.3 Radar basics

1.3.1 Basic principles

Radar stands for radio detection and ranging and originally referred to how radio waves were used to detect and measure the range to objects. The term radar was first used by the US Navy in 1940 (Skolnik 2008). Soon the technique also included the concept of imaging radar, which produced an image instead of mere detection and ranging of objects. Over time radar systems have evolved and today a wide range of frequencies are used, where different sets of pre-defined ranges are called frequency bands. The notations of the bands stem from the earliest use during World War II and can be considered totally random. A few different nomenclatures exist in

parallel; an example of common frequency bands used in remote sensing are listed in Table 1 together with a note regarding their descriptive origin.

The frequency (f) and wave length (λ) are related as $\lambda = c/f$, where c is the speed of wave propagation (the speed of light). The choice of frequency is a vital parameter when designing a radar system, but can often be chosen in such a way that weather conditions like rain and cloud cover can almost entirely be overcome. This is a fundamental advantage of radar systems (active techniques) compared to many other remote sensing technologies that are often limited to using the sun as the only source of radiation (passive techniques). The wavelength is measured in the direction that the wave propagates (*Figure 3*). The orientation of the electric field is referred to as the polarization of the EM wave and the transmitted polarization is determined by the physical structure of the antenna and by its orientation. The EM waves can be transmitted and received in different polarizations (*Figure 4*), where satellite radar systems commonly transmit linear polarizations.

Table 1. *A list of common frequency bands and a brief description of the origin of their names. Adapted from Anon (2003) and Radio spectrum (2014).*

Band name	Frequency range	Wavelength range	Description
VHF	30-300 MHz	1-10 m	Very High Frequency
P	216-450 MHz	0.7-1.4 m	P for "previous"
L	1-2 GHz	15-30 cm	L for "long" wave
S	2-4 GHz	7.5-15 cm	S for "short" wave
C	4-8 GHz	3.75-7.5 cm	C for "compromise" between S- and X-band
X	8-12 GHz	2.5-3.75 cm	X for crosshair (used for fire control)
Ku	12-18 GHz	1.7-2.5 cm	Ku for "kurz-unten"
K	18-27 GHz	1.1-1.7 cm	German "kurz" (short)
Ka	27-40 GHz	0.75-1.1 cm	Ka for "kurz-above"

The principle of radar is that an EM signal is transmitted by an antenna into the surrounding medium, where it is reflected by objects and some of the scattered energy is reflected back to a receiving antenna. In case of the same transmitting and receiving antenna, the radar system is described as "monostatic", when one antenna is transmitting and another receiving, it is described as "bistatic".

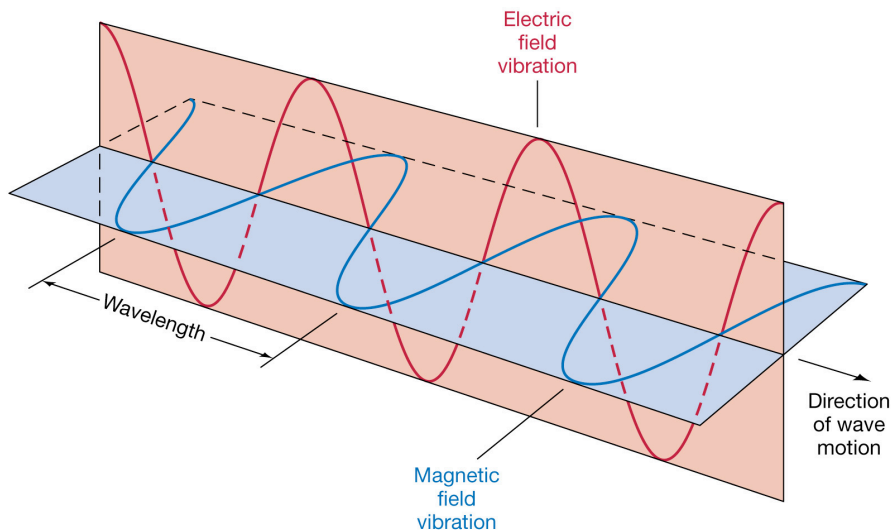


Figure 3. Illustration of an EM wave (Chaisson & McMillan 2003).

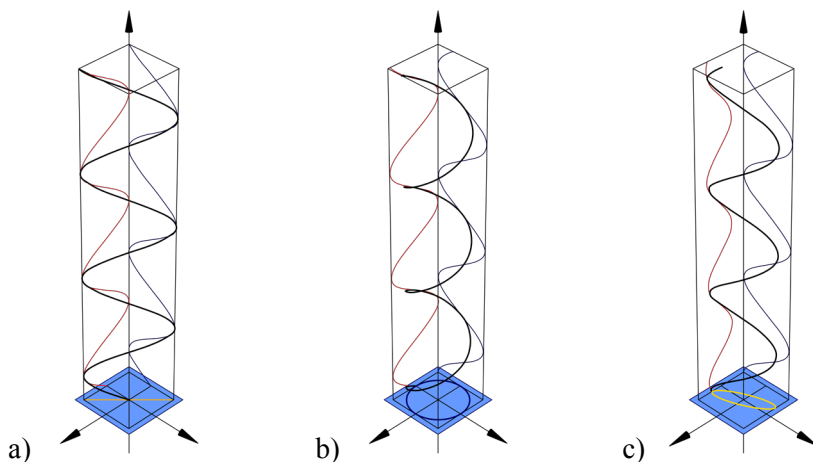


Figure 4. Illustration of polarizations that can be either a) linear (horizontal/vertical), b) circular (right-hand; RHCP or left-hand; LHCP) or c) elliptical.

The ratio of the transmitted power (P_t) and the received power (P_r), stemming from the waves scattered by a target, is commonly called the radar equation (Floyd M. Henderson (Editor) 1998, page 132) and can be written as

$$P_r = \frac{P_t G_t}{4\pi R_t^2} \frac{\sigma A_r}{4\pi R_r^2} \frac{1}{L} \quad (1)$$

where G_t is the gain of the transmitting antenna, R_t and R_r are the distances from the target to the transmitting and receiving antennas respectively, A_r is the effective area of the receiving antenna, L is system losses, and σ is the target's radar cross-section (RCS). The RCS is the only parameter in the radar equation that is related to the target, and depends on the target's physical properties such as size, shape and material. For a perfectly conducting spherical target, the RCS would be equal to the cross-sectional area, πl^2 , assuming l to be the radius of the sphere and with the premise $l \gg \lambda$. While this holds for targets like single trees, remote sensing is often more concerned with entire forests, where the radar system integrates series of radar signals to create 2D images. In this case a more useful measure of the RCS is the radar scattering coefficient σ^o [m^2/m^2], which is defined as the average RCS per unit ground area of the target, and in case of the same transmitting and receiving antenna, it is denoted as the backscattering coefficient.

1.3.2 Resolution of real-aperture radar

The backscattered EM energy can be measured and the distance R to the scattering objects can be determined as

$$R = \frac{cT}{2} \quad (2)$$

where T is the time between the transmission and reception of the radio pulse. The resolution in range ΔR is a measure of the minimum range difference of two objects still resolvable as two single objects and is determined by the length of the (matched filtered) EM pulse. The pulse length is inversely related to its bandwidth B and the range resolution, ΔR_r , can then be written as

$$\Delta R_r \approx \frac{c}{2B} \approx \delta_r \quad (3)$$

An important property of this expression is that the range resolution is independent of range, which makes it ideal for spaceborne platforms as objects at very long distances can be resolved. This also explains why side-

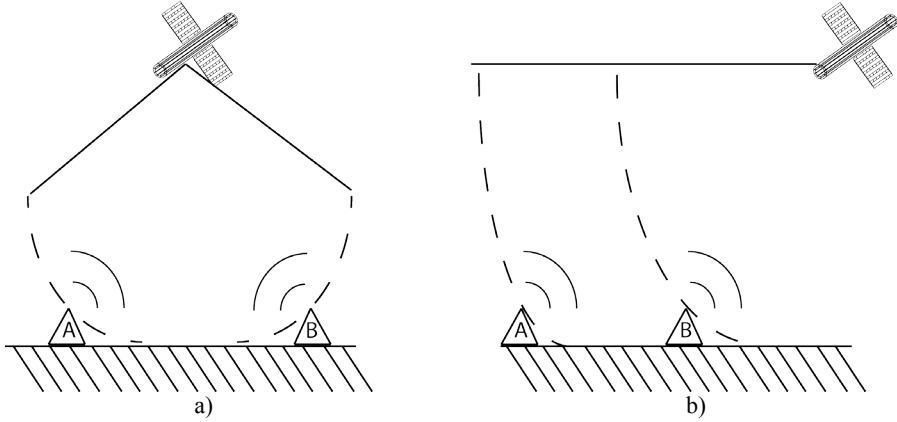


Figure 5. Illustration of a) nadir-looking and b) side-looking configuration. In a) the returns from A and B are ambiguous while the ones in b) are not, because of the separation in time.

looking configurations are preferred over nadir-looking; the former implies that the returns from different scattering objects can be separated using the differences in time, compared to nadir images from which all objects reflect the transmitted EM pulse almost simultaneously (Figure 5).

The antenna pattern expresses the radiation pattern of an antenna where the main lobe of an antenna (=antenna beam width θ) is defined as the 3 dB angle; that is to say that the angular interval having as extremes half of the power with respect to the look direction (Figure 6). The antenna beam width is directly proportional to the wavelength and inversely proportional to the antenna length, L . This can be described as

$$\theta = \frac{\lambda}{L} \quad (4)$$

when $L \gg \lambda$, and is used in the derivation of the azimuth resolution (also called along-track or cross-range resolution).

The azimuth resolution is given by

$$\delta_{az} \approx R\theta_{az} \approx \frac{R\lambda}{L_{az}} \quad (5)$$

where θ_{az} is the beam width and L_{az} is the antenna length (also denoted aperture length) in the azimuth direction. This holds for real-aperture radars, and the azimuth resolution can then only be improved by increasing

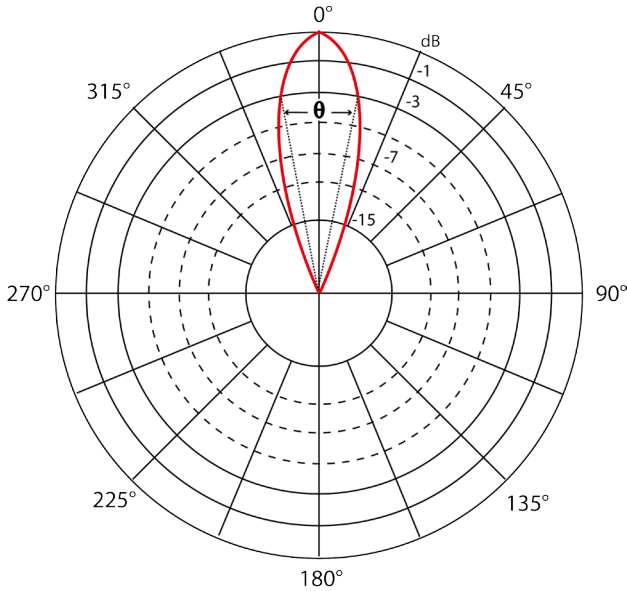


Figure 6. Illustration of the 3 dB angle corresponding to the antenna beam width θ ($\approx 22.5^\circ$ in this illustration) of imaging radar.

the length of the antenna or decreasing the wavelength. Because of the dependence on range, this is not a good solution for remote sensing from long distances and as will be shown in section 1.4.1, another solution is used for the spaceborne case.

1.3.3 Complex electromagnetic signals

A monochromatic EM wave represents the temporal and spatial variations of an electric and a magnetic field in space, which is characterized by amplitude and phase. This can mathematically be represented by a complex number on the form

$$S = Ae^{j\varphi} \quad (6)$$

where A is the amplitude of the wave (expresses the power) and φ is the phase (a value on the $0-2\pi$ interval, defined as $\arctan(\text{Im}(S)/\text{Re}(S))$). The phase is related to the wavelength and is proportional to the distance traveled by the wave, which in the radar case corresponds to the two-way path between the transmitter and the object(s) and can be written as

$$\varphi = \frac{2\pi}{\lambda} 2R = \frac{4\pi R}{\lambda} \quad (7)$$

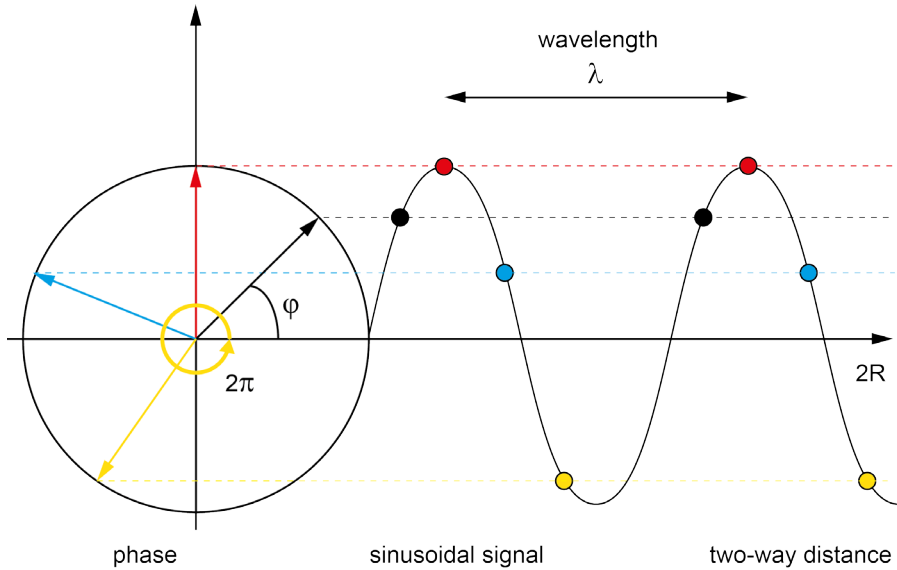


Figure 7. Illustration of a phase-zero transmitted sinusoid, which after travelling the distance $2R$ from the satellite shows a certain phase $4\pi R/\lambda$. Adapted from Ferretti et al. (2007), Fig. 1-5.

Each signal can be represented both in the time (or space) domain and the frequency domain and the relation is given by the Fourier transform, defined as

$$S(f) = \int_{-\infty}^{\infty} s(t)e^{-j2\pi ft} dt \quad (8)$$

where $S(f)$ represents the signal in the frequency domain and $s(t)$ the signal in the time domain. The Fourier transform of a rectangular pulse of length τ is a sinc function where $\text{sinc}(x) = \sin(x)/x$. The difference between the highest and the lowest frequency components is called the bandwidth and in analogy with the definition of the beam width as the 3 dB power loss, the definition $B = 0.89\tau^{-1}$ can be found (Figure 8). This means that a shorter pulse will increase the bandwidth of the signal and a better range resolution can be achieved (recall Eq. 3).

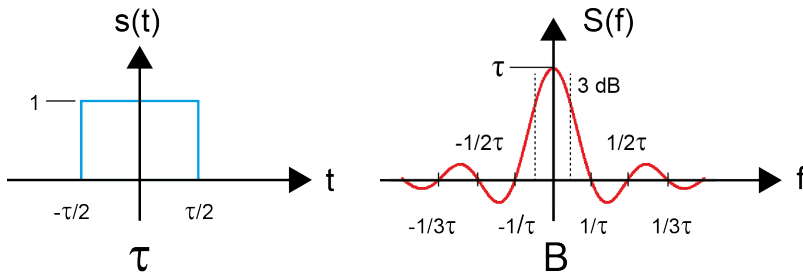


Figure 8. Illustration of how pulse length τ and bandwidth B are related.

The frequency representation of the signal $S(f)$ entails that each signal can be written as the sum of its individual frequency components, and by increasing the number of frequencies transmitted, a larger bandwidth is achieved. In other words, by frequency modulating the pulse (also called chirp signal), a larger bandwidth B of the transmitted pulse is achieved and an increased range resolution is the outcome (Figure 9).

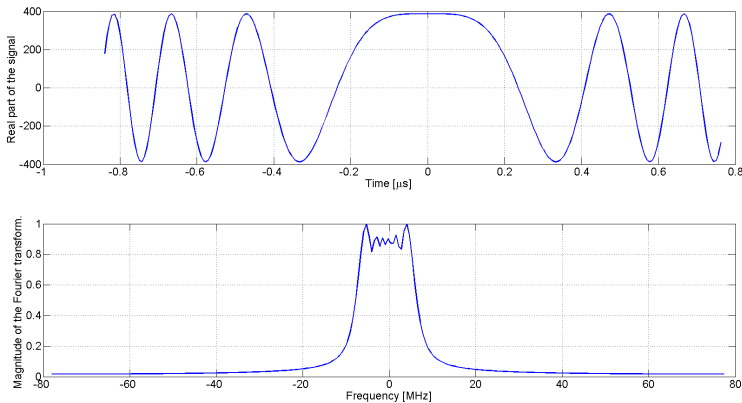


Figure 9. Illustration of a baseband chirp signal in the time and frequency domains. Maximum of the Fourier transform magnitude has been normalized to unity.

1.3.4 Radar scattering

The definition of the backscattering coefficient σ^0 is given to be the RCS per unit area, which can be considered as the sum of the individual scatterers within a resolution cell. This means that when lots of targets within a resolution cell reflect the EM wave at different distances (=phases) from the radar, all reflections will add up coherently to the complex sum of contributions from the individual targets (superposition principle, *Figure 10*). Some contributions will cancel each other out while some will add up, and the coherent sum becomes random on the 2π (or $-\pi.. \pi$) interval. The result of this adding and extinction of phases is called speckle and will appear as “salt and pepper” in the radar images. The random phases originate from the distances between the antenna and the individual scatterers being uniformly randomly distributed on the scale of the radar wavelength (c.f. Smith 1998). The occurrence of speckle causes the amplitude measured from a homogenous area to be Rayleigh distributed, irrespective of the target.

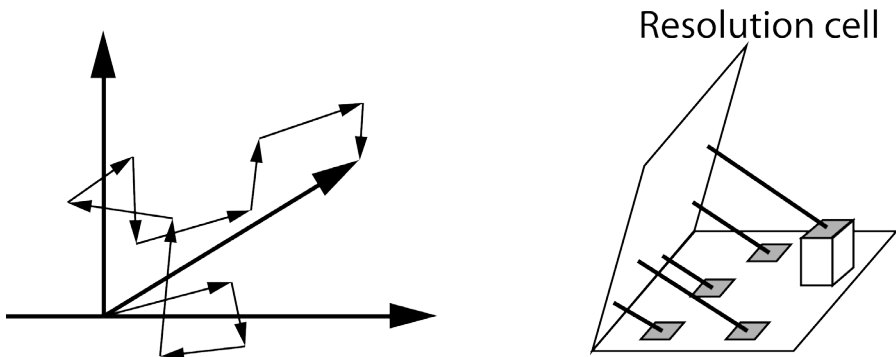


Figure 10. Left: Illustration of how individual scatterers add up to a coherent sum. Right: Illustration of how many different scatterers contribute to the total scattering reflection within a resolution cell.

1.3.5 Geometric effects

The quality of radar images can be affected by the acquisition geometry, which might result in distortion and information loss. The radar “sees” only the line-of-sight, which is called slant range. The radar image is acquired in this geometry, but naturally a “ground range” image is more useful, as it has the Earth as reference and depicts the objects more similar to other geographic data products. Images in slant range will appear compressed in the range direction (*Figure 11*). By knowing the height of the acquisition platform and the incidence angle, correct ground images can be computed by simple geometry; the ground range is simply the projection of the slant range, which corresponds to the slant range divided by the cosine of the incidence angle.

The acquisition geometry might even lead to some information losses, especially in hilly terrain. This is illustrated in *Figure 12*, which shows how the wave front reaches different parts of the ground at different times. In the illustration, the left most parts would normally be expected to be depicted first, but as the actual distance to the top of hill B is shorter than to the base of hill B, this radar echo will return before the echoes from the foot of the hill. This is called layover. Foreshortening is another geometric effect that can occur. This happens when the radar beam reaches the base of a tall feature tilted towards the radar (e.g., mountain A) before it reaches the top. This has the consequence that slopes become compressed in the range direction. Foreshortening and layover are two consequences which result from relief displacement. *Figure 12* shows how the hills B and C are all affected by severe shadowing as well, which means that no radar beams reach the ground and information loss occurs, making it impossible to correctly reconstruct the ground even with advanced signal processing.

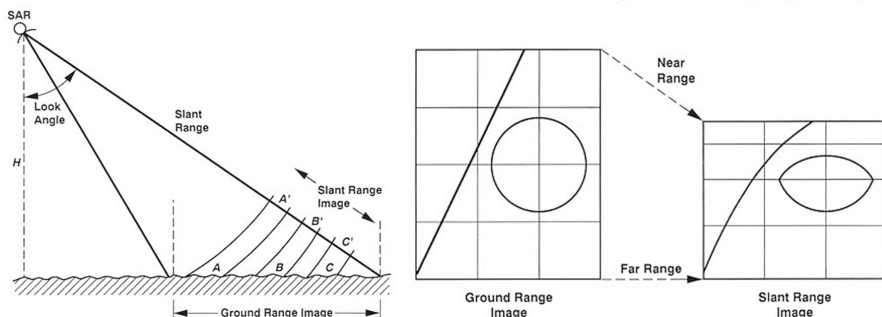


Figure 11. Left: Illustration of how a slant range image translates to a ground range image. Right: Slant range images will appear compressed in the range direction.

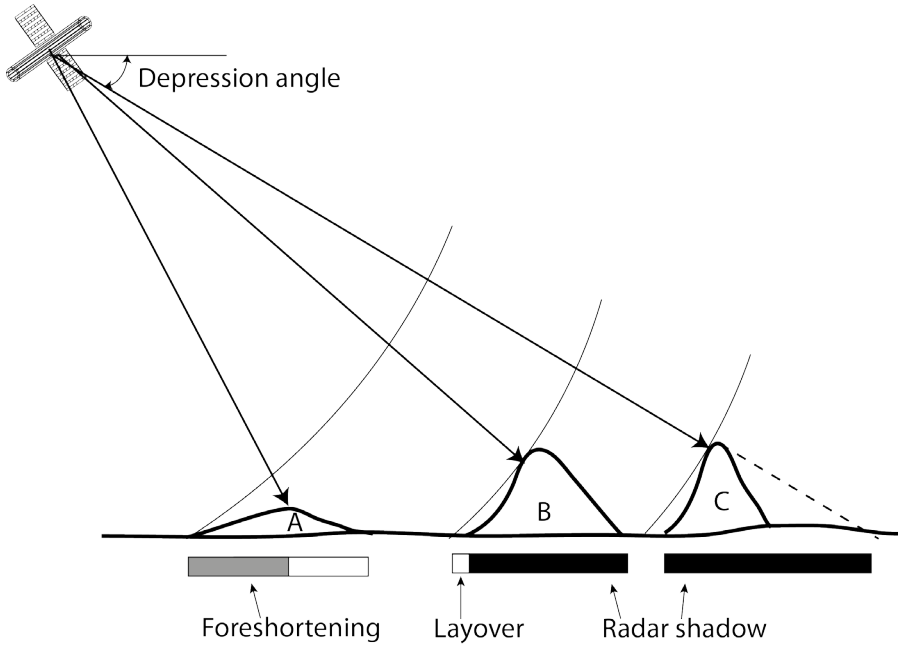


Figure 12. Illustration of geometric distortions caused by the terrain and acquisition geometry.

1.4 Synthetic aperture radar

To retrieve a 2D radar image with high resolution in both azimuth and range direction, a system with high bandwidth and long antenna is needed (Section 1.3.2). To get a reasonable azimuth resolution of a couple of meters or even tens of meters from a spaceborne platform, the antenna needs to be several km long! This is in practice impossible and during the early 1950s the idea of synthesizing a large antenna by moving a smaller antenna along a path emerged (Wiley 1965; Sherwin et al. 1962; Wiley 1985) and Synthetic Aperture Radar (SAR) was invented.

When either the target or the antenna is in motion along the range direction during the acquisition, this can be measured through the rate of change of the phase, which is commonly denoted as the Doppler frequency. The non-relativistic Doppler-frequency shift f_D is given by Ulaby et al. (1982)

$$f_D = -\frac{2dR}{\lambda dt} = -\frac{2v_r}{\lambda} \quad (9)$$

where v_r is the velocity between the target and the radar in the range direction and the other variables have the same definition as previously described.

Consider an antenna mounted on a flying platform, illuminating the ground with the azimuth beam width θ_{az} (Figure 13). An object will then start being illuminated from the transmitted beam as the front of the beam reaches the object. While the flying platform is moving forward, the object will remain within the beam as the platform moves until the rear of the beam is passing the object. The beam is constantly created, as new short radar pulses (chirps) are transmitted over and over at high frequencies. The frequency of the transmitted pulses is called pulse repetition frequency (PRF), and is often on the order of kHz. Each transmitted pulse will bounce against the object and be reflected back to the radar, but as the radar is constantly moving, each pulse will be affected by a different Doppler frequency shift (Doppler Effect, which is the same as can be experienced from the siren of a passing ambulance). The pulse to pulse Doppler shifts can be calculated and by using signal processing, all transmitted pulses that hit the object can be combined coherently. This means that the antenna constituted by the synthetic aperture corresponds to the ground projected length of the azimuth beam width, which thereby allows for a high azimuth resolution as well.

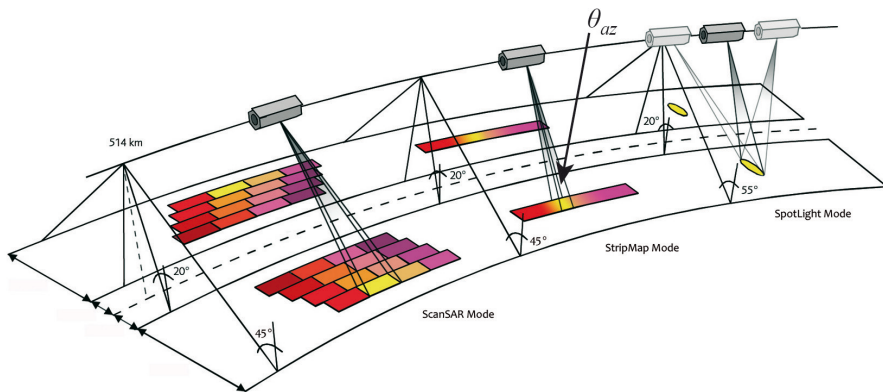


Figure 13. Illustration of the SAR principle for the modes ScanSAR, stripmap (SM) and spotlight (SL) for TerraSAR-X.

1.4.1 Spatial resolution

The azimuth resolution can be described as the capacity of distinguishing between different Doppler frequencies of two neighboring targets along-track. This means that the Doppler bandwidth B_D is given by

$$B_D = |f_{D_max} - f_{D_min}| = 2|f_{D_max}| \quad (10)$$

which is found at the endpoints of the synthetic aperture, if the antenna is aligned against zero-Doppler direction. The diffraction limited resolution is given by Eq. (5), where L_{az} is the antenna length in the azimuth direction. The approximation is valid for $L \gg \lambda$ and hence the Doppler bandwidth can be approximated as

$$B_D = 2|f_{D_max}| \approx \frac{2\theta v}{\lambda} \approx \frac{2v}{L_{az}} \quad (11)$$

where v is the antenna's orbital speed, which in turn gives the azimuth resolution as the time-resolution multiplied by the platform radial velocity. This is approximately the same as the reciprocal of the Doppler bandwidth, which gives

$$\delta_{az} \approx \frac{v}{B_D} \approx \frac{L_{az}}{2} \quad (12)$$

In contrast to real-aperture radar (RAR) systems, the azimuth resolution of a SAR system gets better with a smaller antenna. This is, however, only valid when $L \gg \lambda$ and for a system where the integration angle is limited by the antenna beam width.

The SAR range resolution δ_r (derived in Eq. 3) remains the same as in the RAR system, with the bandwidth B_D as the major limitation of δ_r . In practice, to avoid ambiguities, there is a need of using a higher pulse repetition frequency than the Doppler bandwidth B_D . This translates to an upper limit of the range swath size and also a lower limit on the azimuth antenna size. The lower limit is proportional to the wavelength, so that for long wavelengths large antennas are needed. These constraints by range and azimuth ambiguities hence imply that the swath width and the azimuth resolution cannot be adjusted independently; high azimuth resolution gives a narrow swath and vice versa (Ulaby et al. 1982).

The derivation in this section is valid for stripmap (SM) mode and not ScanSAR or spotlight (SL) mode.

1.4.2 Image characteristics

Radar images acquired with a SAR system differ in a number of ways from the optical images described in Section 1.2. They might at first look similar but optical images are angle resolved in 2 dimensions while the SAR images are resolved only in the azimuth direction. This means that the geometric distortions mentioned in Section 1.3.5, such as layover and shadowing effects, appear in the range direction of SAR images. Furthermore, SAR images are based on EM waves in the microwave region and, generally speaking, three types of scattering can appear (Ulaby & Elachi 1990; Hallberg 2007). First Rayleigh (low-frequency) scattering, where the object size is much smaller than the wavelength, which in this thesis that includes analysis of X-band corresponding to $\lambda \sim 3$ cm, would be the case for the needles and smallest branches. The radiation pattern is typically very broad and rather insensitive to the object shape. Second, resonance scattering takes place when the scattering objects are of similar size as the wavelength. The scattered intensity can fluctuate heavily as the object size changes and this effect is assumed to be less important in forests, as the effect is less evident for objects of lossy material (material that dissipates energy of electromagnetic or acoustic energy passing through it) and there are relatively few objects which match the size of the wavelength as well. Finally, optical (high-frequency) scattering takes place when the objects are much larger than the wavelength. This would especially be the case for the tree trunks and thickest branches.

An example of typical scattering for some common radar bands is illustrated in *Figure 14*. Furthermore, the radar wavelength has the effect that the backscattered intensity in a SAR image is inherently connected to the properties of the target, whereas the brightness in optical images depends on the angle illumination of the sun and radiometric characteristics of the sensor. The radar signature from a target is also connected to the polarization and incidence angle, which, for example, makes SAR images much more sensitive to the surface roughness, as a smooth surface (in relation to the wavelength) would make the incident radar pulses reflect away from the radar rather than get reflected back. This has the effect of producing darker regions in the SAR images.

Finally, SAR images suffer from speckle, which was discussed briefly in Section 1.3.4. This is an effect arising from the EM waves being transmitted and received coherently in a radar system, which makes the phase of the complex amplitude dependent on the distance to the object. When many mutually independent scattering objects are randomly distributed within a resolution cell, the received amplitude is the vector sum

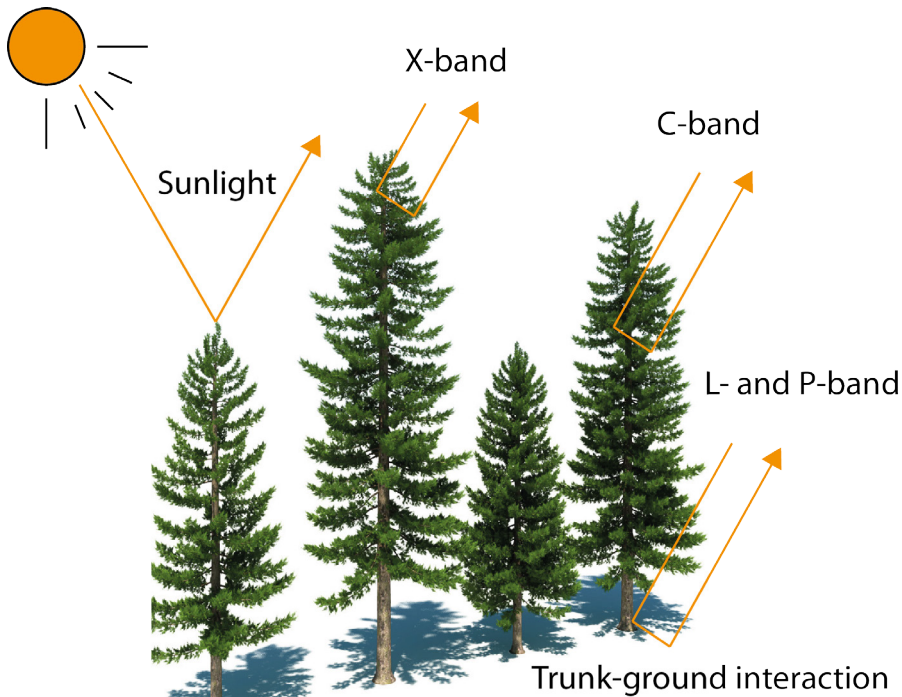


Figure 14. Illustration of the scattering (penetration) in a forest canopy with common remote sensing radar bands. Optical sensors using sunlight are included for comparison.

of all the contributing amplitudes. With sufficiently many scatterers in a resolution cell which are statistically equal, the central limit theorem states that the vector sum obeys a complex circular Gaussian distribution. This means that the value of a single resolution cell is stochastic and the process is known as speckle (Oliver & Quegan 2004).

1.5 Radargrammetry

The term radargrammetry can be deduced from the optical term stereogrammetry but applied to radar images. Its fundamental principle is the stereoscopic viewing of an object from somewhat different angles, which can be related to the perception of depth vision by humans. By combining disparities and convergences, stereo imagery can be attained in our brains. Due to the geometric and radiometric properties of SAR images, which differ from those of optical images (covered in Section 1.4.2), more time is generally required for the eyes to adjust to stereo viewing of SAR images in order to perform visual interpretation. However, depth perception is an active process and object recognition can be trained over time.

In radargrammetry the disparity principle is used to compute the terrain elevation from the measured parallaxes between two images, acquired at different angles (Toutin & Gray 2000). The images are in contrast to InSAR or Polarimetric InSAR (but in similarity to optical photogrammetry) entirely relying on the backscatter intensity of the SAR images. The intensity I , is defined as the amplitude squared, A^2 , and produces an image similar to a black and white photograph.

Radargrammetry was first described in the 1960s by La Prade (1963), who showed that some sets of SAR images could produce similar elevation parallaxes as achieved from aerial images. The topic was further investigated during the following decades by Rosenfield (1968), Gracie et al. (1970), Leberl (1979) and Kaupp et al. (1983). During the 1980s, the SAR systems improved and both same-side and opposite-side stereo viewing were later demonstrated, where the latter was found superior to same-side stereo (Fullerton et al. 1986; Toutin 1996). However, the opposite-side configuration brought severe illumination difficulties, as they got so distinct that despite the geometrical advantages, stereo-viewing became so difficult that the success rate in finding corresponding points and features was limited. An illustration of different system configurations of radargrammetry is shown in *Figure 15*.

Since new launches of different satellite sensors tend to lead to hype over radargrammetry, and in turn lead to research with uneven steps over the years, it should be stressed that same-side configurations have (to the author's knowledge) been preferred and is the primary path the last ~15-20 years of recent research within radargrammetry. In any case, the sensitivity of stereo measurements is increased with increased intersection angles, as the stereo exaggeration factor increases with larger observed parallaxes. This means that larger intersection angles technically give an increased height accuracy of the extracted terrain elevation. On the other hand, as has been discussed, the geometric similarities are important for an appropriate object recognition, which obviously is facilitated by small intersection angles as this gives more identical images. The compromise has often been to use intersection angles in the range of 7-25° and with small temporal differences for the acquisitions, in order to attain suitable geometric parallaxes and smaller radiometric disparities (Kaupp et al. 1983; Mercer 1995; Toutin & Gray 2000; Perko et al. 2011; Persson & Fransson 2014).

Research carried out during the 20th century has mainly accomplished accuracies measured in tens of meters in its best-cases and little attention has therefore been paid to the use of radargrammetry applied to forest. The

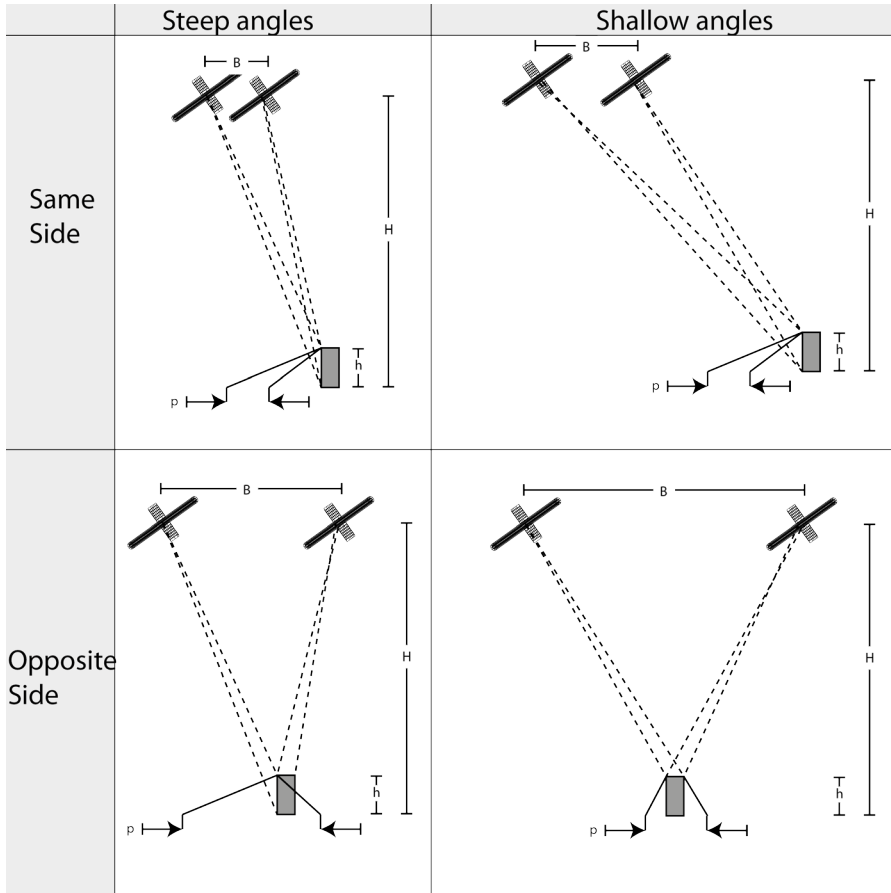


Figure 15. Illustration of different stereo SAR configurations (Toutin & Gray 2000). B=baseline, H=flight height, p=parallax, h=object height.

first noted research on forest canopy height estimation where both radiometric aspects and 3D interpretation from the geometric differences were considered, was carried out by Toutin & Amaral (2000) in tropical forest in Brazil. They estimated canopy height by using relative elevation extraction and compared this to known vegetation maps. The ground level was not known but from clear-cut regions, they could derive relative heights.

The impact of terrain slopes and aspects was studied in Toutin (2002). RADARSAT stereo pairs over three Canadian test sites were processed radargrammetrically to create DEMs, whose accuracies were quantified. The results showed that radargrammetric DEM accuracy was almost linearly correlated with the terrain slopes and that stronger slopes entailed

larger errors. They did not investigate the possible influence of vegetation on the accuracy of the estimations.

In 2007, both the German satellite TerraSAR-X (TSX) and the Italian COSMO-SkyMed were launched. They are both part of larger satellite projects, and with these a new era began where high-resolution radar images from the X-band could be delivered. The spatial resolution is on the order of meters, the geo-location accuracy of the images they deliver is within meters or even less (TSX) and the satellite positioning accuracy is on the order of centimeters (Ager & Bresnahan 2009; Bresnahan 2011; Raggam et al. 2010; Fritz et al. 2008; Schubert et al. 2008; Wermuth et al. 2009). This thesis will not cover COSMO-SkyMed and hereafter only the TerraSAR-X satellite will be discussed in regards to radargrammetry.

The earliest published radargrammetric studies really investigating the inclusion of forest were accomplished primarily by a single research group in Austria (Raggam et al. 2008; Raggam et al. 2009; Raggam et al. 2010; Perko et al. 2011). The main author of the first three studies has been involved in radargrammetry research since the 1980s and has made several significant contributions to the research field. This research group has used a rather technical approach with advanced, well-developed algorithms for image matching and exhaustive error analyses focusing primarily on stipulating actual elevation biases and geo-location accuracies. In Perko et al. (2011), which was an elaboration of Perko et al. (2010b; 2010a), a comprehensive study focusing on radargrammetric extraction of elevations in forests was undertaken. They quantified the EM wave penetration into the forest canopy and evaluated the effect of incidence angle. They combined not only two but three different acquisitions with different intersection angles and the possibilities of performing forest segmentation were evaluated. ALS data were used both for reference canopy heights and as a DTM, which was subtracted to find the height of the radar scattering center. They found that the radar scattering took place at about 70%-75% of the ALS forest height and out of the tested intersection angles, the best DSM quality was achieved from the image triplet (where three different acquisitions were combined). The intersection angles seemed to be indirectly proportional to the resulting DSM quality (i.e., smaller intersection angles resulted in larger standard deviations of the forest height).

At almost the same time, a Finnish research group published the first research on prediction of forest variables at plot-level using TerraSAR-X data (Karjalainen et al. 2012). A nearest neighbor (NN) approach was used where the random forest (RF) technique was applied in the search of

nearest neighbors. They found that the mean forest canopy height could be estimated with 14% RMSE and they also evaluated stem volume, basal area and mean diameter. ALS data were used as known DTM reference and the reference tree heights relied on field measurements.

Radargrammetry was further evaluated in Vastaranta et al. (2012; 2014), where the latter study focused on plot-level estimations of AGB and stem volume. Conformal to Karjalainen et al. (Karjalainen et al. 2012), they used field measurements as reference data, and furthermore the radargrammetric estimations were evaluated against ALS data. They found that the AGB could be estimated with 29.9% RMSE while ALS data led to 21.9% estimation error. Shortly later, in Vastaranta, Niemi, et al. (2014), forest attributes were trained in a most similar neighbor (MSN) estimation approach, using 207 field measured plots, and validated at stand-level using 94 forest stands of mean size 4.1 ha. It was found that H, basal area, stem volume, and AGB could be estimated with 6.7%, 12.0%, 16.3%, and 16.1% RMSE, respectively.

In Solberg et al. (2015), the estimation of AGB from TerraSAR-X SM data using radargrammetry was investigated. The study was carried out on 145 plots (each plot being 250 m²) located in a Norwegian spruce forest. The plot data were also averaged to stand-level and it was found that the AGB could be estimated at stand- and plot-level with 18% and 44% RMSE, respectively. Furthermore, the relationship between CHM and AGB was investigated, and they found this relation to be almost linear. They also compared the estimation accuracy from radargrammetry as a data source with InSAR data. It was concluded that estimations based on InSAR data reached a higher accuracy when a single image pair was used, but that a similar accuracy could be achieved with radargrammetry when two image pairs acquired from opposite directions were averaged.

Despite the intensified interest in radargrammetry over the last five years, more research has to be done in order to quantify different types of errors in different conditions. The technique has not been sufficiently evaluated at different plot sizes and few types of forests have been investigated. The penetration depth is connected to the wavelength used, but the canopy texture also plays a crucial role. Furthermore, none of the presented studies have paid much attention to how humidity affects the conductivity and reflection in the canopy; this can be of great interest when the radargrammetric technique is applied after storms that inherently take place under the worst weather conditions, often with large amounts of precipitation or wet snow. Little research has been undertaken in tropical forest (Lohne 2012), where the forest canopies tend to be significantly

taller than in the boreal forests. Previous research has shown that saturation effects can be a significant problem in all kinds of SAR analysis of forest and this effect is expected to be even more present in dense tropical forest (Imhoff 1995; Neumann et al. 2012).

1.6 Interferometry

A satellite SAR can observe the same area from slightly different look angles by acquiring data from different locations (causing a spatial baseline). This can be achieved from different orbits or like the Shuttle Radar Topography Mission (SRTM), by attaching a 60 m long mast to the space shuttle. It can also be used for observing the same area from the same orbit but by exploiting repetitive acquisitions from different times, creating a temporal baseline. SAR interferometry combines the images acquired at different locations or times, depending on the type of interferometry performed (Bamler & Hartl 1998). When a temporal baseline is used, changes that take place between the two acquisitions can be found. This is useful for measurements of, for example, land subsidence or glacier movements, which often take place at a rather slow pace. Throughout the rest of this thesis, spatial baselines are considered, as long nothing else is stated.

1.6.1 Interferometric phase

Recall from Section 1.3.3 how the EM wave could be described as having both amplitude and phase. This is acquired for each pixel in each respective SAR image from the two satellite sensors (or its corresponding position in case of a single repeat-pass satellite) in interferometric SAR. A so-called SAR interferogram is generated by taking the Hermitian product of the two original complex SAR images, and is therefore a complex image as well. This means cross-multiplying, pixel by pixel, the first SAR image with the complex conjugate of the second. The resulting amplitude is the product of the individual amplitudes whereas its phase (also called interferometric phase) is the phase difference between the images. The following equations in this section are valid for an interferometric configuration with two monostatic SAR systems.

$$\begin{aligned}
s &= g_1 g_2^* \\
&= \left(a_1 e^{-j\varphi_1} e^{-j\frac{4\pi}{\lambda} R_1} \right) \left(a_2 e^{-j\varphi_2} e^{-j\frac{4\pi}{\lambda} R_2} \right)^* \\
&= (a_1 a_2) e^{-j\Delta\varphi} e^{j\frac{4\pi}{\lambda} B_p}
\end{aligned} \tag{13}$$

where s denotes the complex interferogram, g_1 and g_2 are the respective complex SAR images, $*$ denotes the complex conjugate, a denotes the amplitude, φ the phase and R is the distance from the sensor to the respective pixel (target). This requires the images g_1 and g_2 to be co-registered (resampled) at sub-pixel accuracy. The phase is totally random in both SAR images (*e.g.*, from the totally unpredictable scattering manner from twigs and branches in forests), but the phase difference is not because the random effects are to a large degree cancelled out.

To create a SAR interferogram in practice which hence optimizes the magnitude of the mutual coherence corresponds to the complex correlation coefficient $\tilde{\gamma}$ being defined as

$$\tilde{\gamma} = \frac{E[g_1 g_2^*]}{\sqrt{E[|g_1|^2] E[|g_2|^2]}} \tag{14}$$

where E represents the expectation value operator (Born & Wolf 1980). The phase $\hat{\varphi}$ is then given by the argument

$$\hat{\varphi} = \arg \left(\sum_{i=1}^N g_{1,i} g_{2,i}^* \right) \tag{15}$$

where N is the number of pixels in the estimation window.

The distance between the two satellites (or orbits) in the plane perpendicular to the orbit is called the interferometric (or parallel) baseline B_p and its projection perpendicular to the slant range is the perpendicular (or normal) baseline, B_{\perp} . This geometry is illustrated in *Figure 16*.

Assume only one dominant point scatterer in each ground resolution cell that does not change over time. The interferometric phase will then be a result from the pure difference in travelling path between the two sensors. This difference can then be approximated as

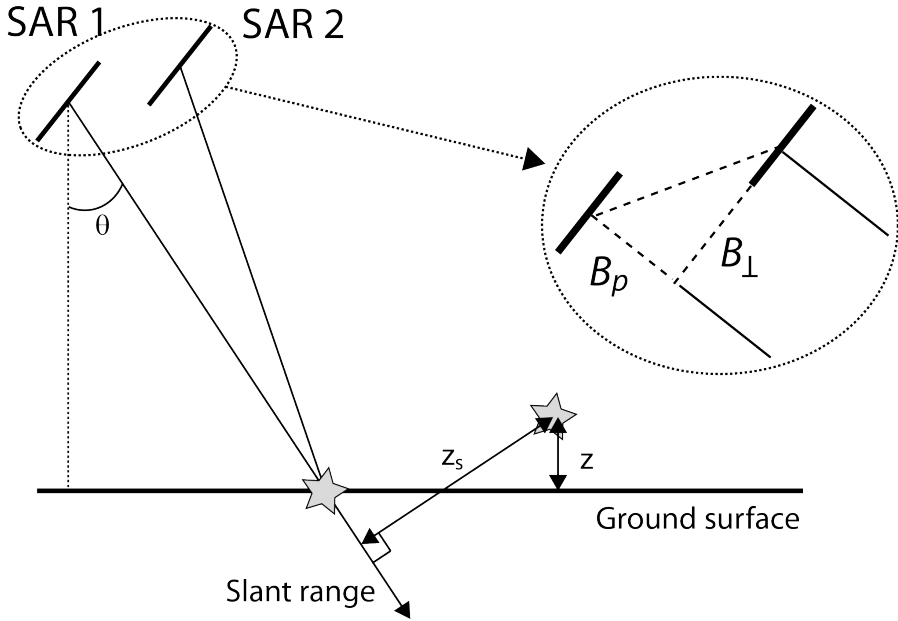


Figure 16. Illustration of the geometry of satellite interferometric SAR system.

$$\Delta R = \frac{B_{\perp} z_s}{R} \quad (16)$$

where z_s denotes the displacement between the resolution cells along the perpendicular to the slant range. This assumes co-registered acquisitions.

The interferometric phase variation $\Delta\phi$ is then proportional to ΔR divided by the transmitted wavelength λ :

$$\Delta\phi = \frac{2\pi\Delta R}{\lambda} \quad (17)$$

It is rarely the case that each resolution cell contains only one scatterer and as this thesis focuses on forest, this will be discussed further. With many scatterers present, the resolved phase will be influenced by noise resulting from the different scatterers' contribution. First the atmospheric contribution should be mentioned, which can be the result of atmospheric humidity, temperature and pressure differences between the two acquisitions. As this thesis only deals with acquisitions from a bistatic configuration which means simultaneous acquisitions with relatively small baselines, the atmospheric influences can be neglected. Another error

source can be due to temporal changes of the scatterers. In forest, it is likely that the trees are swaying in the wind and therefore change their position within a fraction of a second. Because of the bistatic setup though, this error source should again be minor or even non-existing (if the along-track baseline is 0, otherwise the individual acquisition focusing at different zero-Doppler positions causes a minor temporal decorrelation). Furthermore, slightly different look angles from the satellite sensors cause differences in the RCS of the individual scatterers in a resolution cell. It indirectly depends on the terrain slope and this phase term can often be removed from the interferogram thanks to common band filtering (also called spectral shift; Ferretti et al. 2007). An important consequence of the effects resulting from different look angles is that there exists a critical baseline over which the interferometric phase is pure noise and cannot be removed. Last but not least, there can be a significant phase noise due to volume scattering (e.g., the canopy with its branches of a tree). The speckle changes depending on the penetration depth into the canopy and is discussed further in Papers IV and V.

1.6.2 Height of ambiguity

The height difference generating an interferometric phase change of 2π has been defined as height of ambiguity (HOA). This gives an intuitive understanding of the sensitivity that can unambiguously be resolved by the interferometric system and it is inversely proportional to the perpendicular baseline

$$\text{HOA} = \frac{\lambda R \sin\theta}{2B_{\perp}} \quad (18)$$

This expression is valid for a monostatic system configuration, while for the bistatic case (that is used throughout this thesis), a factor of 0.5 must be added to adjust for the travel path being half of the monostatic case. As a rule of thumb, the longer the perpendicular baseline, the more accurate the altitude measurement since the phase noise correlates to smaller altitude noise. The drawback is that longer baselines cause the phase noise to increase because of the increased difference in look angles and the coherence becomes zero above the critical baseline.

1.6.3 Interferometric coherence

The coherence estimate is the magnitude of the complex correlation, denoted

$$|\tilde{\gamma}| = \frac{|(\sum_{i=1}^N g_{1,i} g_{2,i}^*)|}{\sqrt{\sum_{i=1}^N |g_{1,i}|^2 \sum_{i=1}^N |g_{2,i}|^2}} \quad (19)$$

with the assumption that an ML estimator is used. The coherence describes the interferogram quality (SNR) and takes a value on the [0..1] interval, where 0 means that the phase is only noise while 1 implies perfect coherence. The selection of the window size is essential for the InSAR coherence image. With only one pixel as the window, the coherence is equal to unity but without meaning, so by choosing a larger window, this estimation bias decreases. The ML estimator is valid only for statistically independent samples, which hence implies that the number of physical looks (pixels) is not the same as the number of independent looks. The exact relation between the interferometric phase dispersion σ_φ and coherence can be found through complicated mathematical computation. However, if the number of looks (NL) is greater than four, then independent pixels with the same coherence are averaged and the following simple approximation holds (Rosen et al. 2000)

$$\sigma_\varphi = \frac{1}{\sqrt{2NL}} \frac{\sqrt{1 - \gamma^2}}{\gamma} \quad (20)$$

1.6.4 Theoretical relationships between InSAR and forest parameters

The coherence can be split into different factors (c.f. Hagberg et al. 1995)

$$\gamma_{total} = \gamma_{processor} \gamma_{noise} \gamma_{temporal} \gamma_{spatial} \quad (21)$$

which are approximately the same components as discussed in Section 1.6.1 about phase error sources. The first term, $\gamma_{processor}$, descends from the processing chain that forms the interferogram. This term could also include co-registration decorrelation. This chain is nowadays efficiently developed and the TanDEM-X co-registration has sub-pixel accuracy, hence, this term can be neglected. The second term, γ_{noise} , is related to the fact that in regions with low backscatter, the coherence will be reduced because the noise in the different acquisitions is decorrelated. In the case of TanDEM-X

data, the coherence over forest and open land is consistently sufficient and this term can also be neglected. The third term, γ_{temporal} , comes from temporal decorrelations, which are principally zero in the bistatic configuration of TanDEM-X. The last term, γ_{spatial} , refers to the incidence angle differences of the two receivers relative to the target. This term can be split into two, described as $\gamma_{\text{spatial}} = \gamma_{\text{volume}}\gamma_{\text{range}}$, where γ_{range} depends on the baseline and on the range dimension of the resolution cell. In the special case of surface scattering (limited to a single plane), the range decorrelation can be compensated by wavenumber filtering (Gatelli et al. 1994). In the case of forests, the scattering function is no longer limited to a plane but is a function of the height above the ground plane (i.e., the scattering is spatially homogenous in the horizontal plane). After wavenumber filtering, the residual decorrelation can be written as a Fourier transform of the height distribution of the temporally stable backscatter (Ulander & Hagberg 1995; Hagberg et al. 1995; Cloude & Papathanassiou 2003; Mette 2007), such that

$$\gamma_{\text{spatial}} = \gamma_{\text{volume}} = \frac{\int \sigma_z e^{-j \frac{4\pi B_{\perp}}{\lambda R \sin \theta} z} dz}{\int \sigma_z dz} \quad (22)$$

where σ_z is a function describing the vertical distribution of scattering. This is fundamental for the biophysical models covered in this thesis and they are discussed further in Papers IV and V.

1.6.5 Interferometric Water Cloud Model

A simple model that attempts to describe forest parameters' relationship to forest backscatter was presented by Attema & Ulaby (1978). This model is based on radiative transfer theory and assumes a homogenous vegetation layer made up of random scatterers. They built their theories on the fact that the microwave dielectric constant of dry vegetative matter is much smaller than the dielectric constant of water. Furthermore, the forest canopy is usually composed of more than 99% air by volume, which made them propose that the canopy can be modeled as a water cloud, with its droplets being held in place by the vegetative matter. This theory assumes identical droplets that are randomly distributed within the canopy and therefore the scattering and attenuation cross-section contributions can be modeled, presuming N droplets per unit volume. The total contribution from the vegetation is the incoherent sum of the energies scattered at each layer. In case of high vegetation density, the attenuation along its path into the canopy will increase and the major part of the reflection will come from the

canopy, giving a negligible ground contribution to the total backscatter. This will lead to saturation effects due to the absence of scattering from the underlying canopy structures and thus affect the total backscatter. Longer wavelengths currently seem to be the only solution to this problem.

The idea of using this model was further tested and proposed by Hagberg et al. (1995), Ulander & Hagberg (1995), Richards et al. (1987), Pulliainen et al. (1994), and Fransson & Israelsson (1999), and for the first time the “Interferometric Water Cloud Model” (IWCM) was introduced in Askne et al. (1995; 1997) and Askne & Smith (1996). It was fully described in Dammert (1999), Santoro et al. (2002) and Askne & Santoro (2003).

The IWCM is essentially the same idea as originally presented by Attema & Ulaby (1978), in that the IWCM also expresses the total forest coherence (*for*) as a sum of two contributions coming from the vegetation (*veg*) and the ground (*gr*). The vegetation scatterers cover a certain fraction of the total area, denoted area-fill factor η , and the vertical scattering profile is an exponential function described by an attenuation coefficient α . The IWCM model can be written as

$$\gamma_{for} = (1 - \eta)\gamma_{gr} \frac{\sigma_{gr}^0}{\sigma_{for}^0} + \eta \left[\gamma_{gr} \frac{\sigma_{gr}^0}{\sigma_{for}^0} T_{tree} + \gamma_{veg} \frac{\sigma_{veg}^0}{\sigma_{for}^0} \left(\frac{\alpha}{\alpha - j\omega} \right) (e^{-j\omega h} - T_{tree}) \right] \quad (23)$$

where σ_{for}^0 is the forest backscatter and T_{tree} represents the two-way transmissivity through the tree canopy (as presented in Askne et al. 1995). Further σ_{for}^0 is defined as

$$\sigma_{for}^0 = (1 - \eta)\sigma_{gr}^0 + \eta[\sigma_{gr}^0 T_{tree} + \sigma_{veg}^0(1 - T_{tree})] \quad (24)$$

and ω is the InSAR system geometry coefficient

$$\omega = \frac{4\pi B_{\perp}}{\lambda R \sin\theta} = \frac{2\pi}{HOA}. \quad (25)$$

The IWCM can despite its length and complex look be accepted as a reasonably simple model. It takes into account the vegetation contribution and the ground contribution, both from direct scattering through gaps in the canopy and from the attenuated signal making it all the way through the

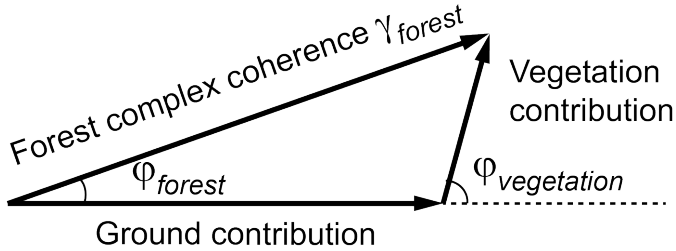


Figure 17. Illustration of the total forest complex coherence in terms of a real vector (ground contribution) and a complex vector (vegetation contribution) that includes volume decorrelation and InSAR effects (Santoro 2003).

canopy and then reaching the ground and back to the sensor. Under the assumption that volume decorrelation is the only source of decorrelation, it is possible to invert forest heights from the complex coherence.

1.6.6 Random Volume over Ground

While IWCM models the volume decorrelation as a function of both the scatterer distribution in height and the gaps in the horizontal direction, a slightly less complex approach, Random Volume over Ground (RVoG), was presented by Treuhaft et al. (1996). It still models the forest as a decorrelating volume of randomly distributed scatterers but the gaps are excluded. The scatterers are located at height h but the uniform scattering profile is slightly changed by introducing an extinction parameter α . The ground is modeled as non-decorrelating and gives a definite backscatter contribution.

It is not possible to invert these parameters (height, extinction and ground) from a single complex coherence image because of the underdetermined system setup. Options to include more data in order to solve for all variables are to use more baselines, frequencies or polarizations.

RVoG models have been evaluated using multiple baselines in Treuhaft (2002), multiple frequencies in Dutra & Elmiro (2002) and Wheeler & Hensley (2000), and multiple polarizations by using polarimetric InSAR (Pol-InSAR) data in Treuhaft & Siqueira (2000), Papathanassiou & Cloude (2001) and Cloude & Papathanassiou (2003). The power and InSAR sensitivity to tree height and vegetation density were compared in Treuhaft & Siqueira (2004). Out of the options to include more data, the frequency option is restricted by the available satellite sensors providing data. Therefore, it can be expected that variations of the baseline and polarizations are more commonly researched, and the latter has frequently

become the most accessible option. This is, of course, most in line with how RVoG first was presented: as a model used with Pol-InSAR data (Treuhaft et al. 1996).

Following from the definition of volume scattering (Eq. (22)), the total backscattering σ_V^0 in RVoG can be described as the sum of the effective ground σ_{gr} and volume σ_V backscattering after extinction (Papathanassiou & Cloude 2001; Cloude & Papathanassiou 2003):

$$\sigma_V^0 = \sigma_{gr} + \sigma_V = \sigma_{gr'} e^{-2\alpha h} + \int_0^h \sigma_{V'} e^{2\alpha z} dz \quad (26)$$

and letting the ground-to-volume ratio m be described as

$$m = \frac{\sigma_{gr}}{\sigma_V} \quad (27)$$

then the complex coherence from the volume can be written as

$$\gamma_{Vog} = \frac{m + \gamma_{volume}}{m + 1} = \gamma_{volume} + (1 - \gamma_{volume}) \frac{m}{m + 1} \quad (28)$$

The reason for the last paraphrasing in Eq. (28) is that it makes it easier to interpret geometrically (*Figure 18*), which gives significance to the model as it can be more easily fitted to experimental observations. As can be seen both in *Figure 18* and Eq. (28), the extent of observable coherence is described as a straight line in the complex plane going through the point γ_{volume} with direction $(1 - \gamma_{volume})$. The origin of the line is located at the ground phase on the unit circle, where $m = \infty$ and ends where $m = 0$, which corresponds to volume decorrelation only. The length depends on the baseline, radar frequency, height and mean extinction of the vegetation layer and the amplitude of the ground scattering mechanisms (Papathanassiou & Cloude 2001).

Recall that γ_{volume} describes the relation between the interferometric coherence and the scatterer height distribution σ inside a resolution cell. This is commonly chosen as an extincted scattering profile, which means that as the radar wave penetrates the volume, the backscatter will be more and more attenuated the further into the volume it travels. For a constant extinction along the volume depth, the backscattering coefficient σ^0 becomes an exponential function of the extinction α and the 2-way penetration through the height h of the volume

$$\sigma^0 = \text{const} \int_0^h e^{2\alpha z / \cos\theta} dz. \quad (29)$$

The extinction in the volume is assumed independent of polarization while the ground contribution changes with polarization. Their contributions act as antagonists where increased extinction displaces the scattering center towards the canopy top with increased coherence as a direct consequence. When instead the ground contribution increases, the scattering center is shifted down towards the vegetation floor which gives lower coherence as a result (except for high ground contributions).

When RVoG has been implemented with the polarization approach, each of the three polarizations HH, VV and HV=VH provide coherence and phase, for a total of six parameters. These are values (complex images) that can be obtained from a typical InSAR system. The corresponding six unknown parameters in the RVoG model to be found are height (h), extinction (α) where $\alpha_{HH}=\alpha_{VV}=\alpha_{VH}$, ground contributions ($m_{HH} \neq m_{VV} \neq m_{VH}$) and ground phase (φ_0). To avoid ambiguities during the model inversion, the coherence most distant from the ground phase is often assumed to have no ground contribution, i.e. $m=0$ (Mette 2007). For a complete description of the inversion procedure and discussions about problems and corrections this has been examined thoroughly in Papathanassiou & Cloude (2001), Cloude & Papathanassiou (2003) and Mette (2007).

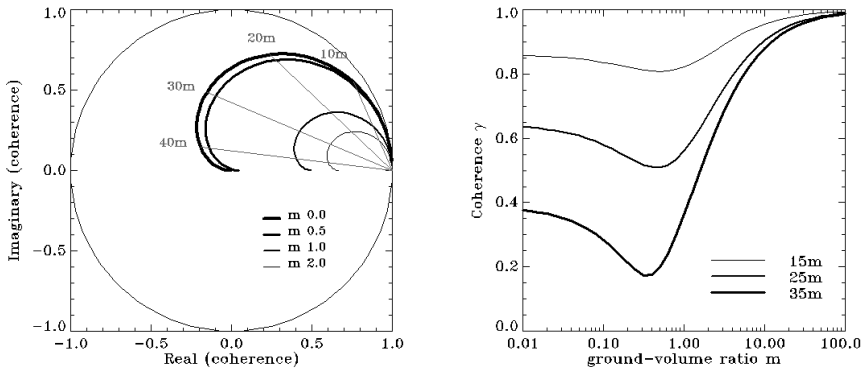


Figure 18. Geometrical interpretation of the RVoG scattering model (Mette 2007, Fig. 3-17 c and Fig. 3-18 b). Left: The complex coherence is dragged towards the ground phase. Volume heights from 10-40 m are indicated. Right: Effect of ground on the coherence-height relation.

1.6.7 Forest research based on InSAR

InSAR has long been used for retrieval of height information as demonstrated by Li & Goldstein (1990), who tested the feasibility to use repeat-pass SEASAT InSAR data for topography measurements. In addition to DTM generation, differential interferometry (D-InSAR) has efficiently been applied for detection of fine changes in topography, such as glacier motion, land subsidence or earth quakes (Goldstein et al. 1993).

InSAR has been applied to forestry for classification and estimation of forest related variables like basal area, tree height, biomass and stem volume. Wegmüller & Werner (1995; 1997) evaluated interferometric signatures to discriminate forest from other land categories and Hagberg et al. (1995) evaluated the coherence and interferometric height in regions of forest. Backscatter based methods have shown significant signal saturation effects, already at 20 tons ha⁻¹ for C-band, and is hence a limited option for most forestry applications (Imhoff 1995). Semi-empirical models based on simplified physical reasoning, such as IWCM or RVoG, in combination with more empirical approaches that use the interferometric height, have become the most researched alternatives. Askne et al. (1999), Santoro et al. (2002), Askne et al. (2003) and Santoro (2003) have evaluated the IWCM model for ERS C-band data for estimation of tree height, biomass, and stem volume. Papathanassiou & Cloude (2001) evaluated the RVoG model for L-band SAR data for forest height estimations.

An empirical approach was tested by Rombach & Moreira (2003), where the interferometric height difference between P- and L-band data from OrbiSAR-1 was used to model the canopy height in tropical forest in Brazil. Similarly Neeff et al. (2005) used airborne InSAR from X- and P-band to monitor biomass in the Brazilian Amazon. By using interferometric height in combination with P-band backscatter, they reached a precision of $r^2=0.89$.

In Izzawati et al. (2006), X-band InSAR data were modeled with a coherent backscatter model and compared to Intermap data for coniferous plantations in the UK. The most important results showed that crown shape, tree density and tree height are vital in the process of height retrieval. Variation in viewing angle and terrain slope (<30°) did not affect the height retrieval much. The finding that tree density also influences the measured canopy height is interesting and deserves further investigation, as the tree height is not influenced by tree density (Solberg et al. 2013; Solberg et al. 2015).

The relation between airborne X-band InSAR data and ALS forest height was further evaluated by Balzter et al. (2007), who found the mean

stand height obtained from InSAR to be comparable with heights observed from ALS data and field measurements, with an RMSE of 2.5 m. They also noticed that the estimation of tree top heights was more sensitive to gaps in the canopy than the estimation of the mean height (canopy height), possibly because of the significant ground contribution and also side hits into nearby standing trees.

A polarimetric InSAR (Pol-InSAR) approach for forest height inversion was tested with airborne P- and L-band data in Hajnsek et al. (2008). Garestier et al. (2008) inverted airborne X-band Pol-InSAR data from the HH and HV channels with an RVoG model to represent the forest height of a sparse pine forest. Furthermore, they noticed a significant height difference (~6 m) between the polarizations and that inversion at X-band was not very sensitive to different values for mean extinction, which vouches certain robustness for the RVoG approach. They found that the RVoG inversion was more sensitive to the forest density, especially at X-band compared to lower frequencies, and that the inversion was easier in sparser forest. With denser forest, fully polarimetric data could possibly be a satisfactory approach. P- and L-band data from airborne systems were tested for biomass estimations in Hajnsek et al. (2009), where focus was put on tomography, which is 3D acquisitions from different baselines. A follow-up to Hajnsek et al. (2008) was presented by Ulander et al. (2010), in which Pol-InSAR was acquired at P-band for biomass estimations as well as forest changes in hemi-boreal southern Swedish forest. By using the same test site and data from more than a three years' time span, they had a unique opportunity to study forest changes and their effect on radar observations.

In Solberg et al. (2010), InSAR data from the shuttle radar topography mission (SRTM) in 2000 were used in an empirical approach to estimate Norway spruce and Scots pine biomass from the interferometric height. They found a linear relationship between AGB and the interferometric height, with 19% RMSE at stand-level. No saturation effects were noticed, which is in agreement with the earlier studies making use of the interferometric height. In addition, they noticed a parametrical difference between spruce and pine where spruce had a higher biomass increase in tons ha⁻¹ compared to pine.

Caicoya et al. (2012) used TanDEM-X InSAR data to model biomass at the Swedish test sites of Remningstorp and Krycklan, by implementing an RVoG model. They found a high sensitivity for biomass classification based on four biomass classes, up to 250 tons ha⁻¹. They also concluded that longer baselines (=lower *HOA* values) were more sensitive to low

biomass levels and that longer baselines could possibly complement the classification for a better full spectra, at both low and high biomass levels. The baseline sensitivity was evaluated at the same test sites in Soja & Ulander (2013), who found that baselines corresponding to *HOA* values in the order of 50-80 m were preferred for CHM estimations in the forest found at these test sites.

In Praks et al. (2012), the scattering phase center (SPC) location for airborne X- and L-band data in boreal forests was investigated. For X-band, the SPC was typically about 75% of the canopy height (measured with ALS), which is in line with Perko et al. (2011) who suggested 70%-75%. An RVoG model was applied and they found that at X-band, the ground contribution could most likely be assumed negligible for canopies possessing tree heights exceeding 10 m. Compared to ALS height measurements the RMSE was close to 1.5 m in homogeneous regions. Hurtado (2012) evaluated this approach with TanDEM-X InSAR data and found the R^2 to be 0.62 for the interferometric forest height estimation of ALS height.

The performance of biomass estimation from Pol-InSAR data was tested in Neumann et al. (2012). Airborne P- and L-band data were used with an RVoG model approach at the Swedish test site Krycklan and the most successful estimations were found with L-band data. It was found that the intensity at HH-VV was more sensitive to biomass than any other polarization at L-band. In contradiction to some earlier reported studies, it was also found that the incidence angle and topography dependence had a large impact on the results. This might be due to the fact that P- and L-band data were utilized, where the ground contribution and therefore its topography becomes more pronounced.

In Solberg et al. (2013), TanDEM-X InSAR data were used to evaluate the interferometric height sensitivity to spruce tree volume and biomass. They found the stem volume and AGB to be proportional to the interferometric height, with 19-20% RMSE at stand-level. A crucial finding in this study was the possibly linear relation between the interferometric height and stem volume, as this stands in contradiction to earlier studies claiming curvilinear relationships (Askne et al. 1997; Mette et al. 2004; Woodhouse 2006). A possible explanation given was that stand volume and AGB might be linearly related to the canopy height while it could be curvilinearly related to the mean tree height and top height (H_{100} ; recall Section 1.1.1).

Shortly later Askne et al. (2013) compared IWCM, RVoG and a penetration-depth (PD) model for AGB estimations from TanDEM-X data.

They found the RMSE to be between 17% and 33% at stand-level with IWCM, 17% and 40% with RVoG and 18% and 33% with PD. Their results validated the finding by Solberg et al. (2013), however this should be evaluated in a wider range of environmental conditions.

Spaceborne SAR systems rarely offer fully Pol-InSAR data but rather “compact” Pol-InSAR with, for example, only two polarizations. Arnaubec et al. (2014) evaluated the precision of vegetation height estimations when an RVoG model was applied to P-band data at different or many polarizations. It was found that a loss in vegetation height precision could be calculated, independent of estimation method, when derived from an adaptation of the Cramer-Rao bound. It is possible that a similar theoretical derivation could be done for X-band data.

The performance of “compact” Pol-InSAR with TanDEM-X data was thoroughly tested in Kugler et al. (2014), where forest height was the primary estimated parameter. They evaluated single- and dual-polarization cases against ALS forest heights by applying a two-layer RVoG model, at the test sites Krycklan (in northern Sweden), Traunstein (in southern Germany) and Mawas (a tropical test site in Indonesia). The lowest RMSE was found at the Swedish test site, with 1.58 m and with $r^2=0.91$ for the single-polarization inversion. The dual-polarization inversion was noisier but still had an RMSE=2.02 m and $r^2=0.86$. They noticed a topographic influence on the inversion performance at the Krycklan test site. It was concluded that the correlation between the SPC and tree top was strong but varied with seasonal and environmental changes. They only noticed weak effects of the incidence angle on the penetration, but in general the penetration was surprisingly high for being from X-band. It was not made clear if the deep penetration was due to actual penetration through the vegetation volume or due to gaps in the vegetation layer.

1.7 Concluding remarks

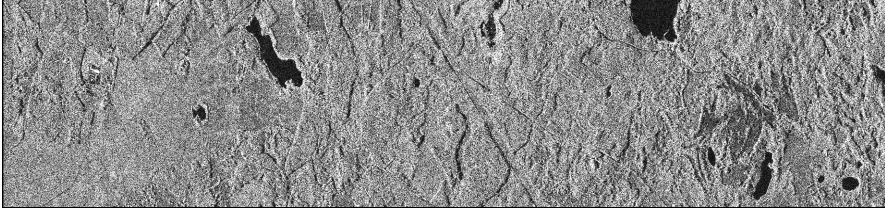
The remote sensing techniques covered in this thesis possess different advantages. Yet there is more research to be done as these techniques have not been fully investigated. All of the techniques covered in this thesis also assume that an accurate DTM is available. In brief, the current status for each technique used in this thesis is given below.

Optical satellite images that are used for AGB and H estimations have their strength in the relatively high resolution images and rather robust radiometric quality of the acquisitions, which enables solid estimations. Drawbacks are that these are based on passive remote sensing techniques,

which require daylight and cloud-free acquisitions, and also have signal saturation at higher biomasses. The satellite based stereogrammetric technique has not yet been thoroughly investigated for forestry applications.

Radargrammetry can provide necessary images at any time of the year and is little affected by changing weather conditions. The quality of the images is relatively high but the demands on suitable images are also high, which restricts operational use of this technique. Estimations with radargrammetric data sources are strongly affected by topography and should be further investigated at different plot sizes, weather conditions (especially frozen/unfrozen), polarizations, and wavelengths. The possible saturation effect should be investigated at higher biomasses. The canopy penetration of radar waves needs detailed examination at different wavelengths and forest types.

Interferometric SAR based methods possess the same advantages as radargrammetry, with imagery accessible all-year round, but has less strict requirements on baselines. In this thesis only TanDEM-X data were used and therefore basically every revolution could provide usable InSAR data. The image quality is high but for operational use around the globe, the energy supply could be a potential problem for keeping the sensors in acquisition mode at all times. InSAR based estimations of forest variables seem to be less influenced by topography than radargrammetry at X-band, but especially in sparse boreal forest where the ground exposure can be expected to be high, this assumption should be further investigated. The precise information content in the interferometric height is not dissolved, but includes both tree height and forest density data. InSAR images are of high quality and both single-tree and forest density methods are of interest for future development and evaluation.



2 Objectives

The main objective of this thesis is to evaluate different techniques using 3D satellite data for estimation of forest parameters, primarily AGB and H in boreal forests. The specific objectives for Papers I-V are

- I To find out whether an improvement of AGB and H estimation could be achieved by adding height metrics from a CHM derived from optical along-track satellite data to multispectral data from SPOT-5 HRG.
- II To evaluate the potential of using radargrammetry with TerraSAR-X images for estimation of AGB and H at stand level.
- III To evaluate the potential of replacing ALS data with TanDEM-X InSAR data for operational use in order to estimate AGB and H in boreal forest. Furthermore, the effects of forest density and scale were evaluated.
- IV To introduce a two-level model suitable for estimation of both forest height and canopy density through model inversion from one ground-corrected InSAR complex correlation coefficient.
- V To introduce a model for AGB estimation from InSAR data based on the two-level model used to estimate forest height and canopy density. Additionally, to provide a simplified and more robust version of the model suitable for AGB estimation in regions where little or no training data are available.



3 Materials and methods

3.1 Materials

3.1.1 Test sites

The test sites used in this thesis were located in Krycklan and Remningstorp (*Figure 19*). Krycklan is an approximately 7,800 ha large catchment area in northern Sweden (Lat. 64°16'N, Long. 19°46'E). It consists of approximately 6,780 ha managed boreal forest dominated by Norway spruce (*Picea Abies*), Scots pine (*Pinus Sylvestris*) and birch (*Betula* spp.). The region is moderately hilly and the elevation varies between 125 and 350 m.a.s.l.

The Remningstorp area is a production-managed boreal forest in southern Sweden (Lat. 58°30'N, Long. 13°40'E) consisting of about 1,600 ha land, of which about 1,200 ha are forested with Norway spruce, Scots pine and birch as the dominant species. The region is flat with elevations between 125 and 145 m.a.s.l.

Papers I and IV had Remningstorp as a test site while Papers II, III and V used both Krycklan and Remningstorp. Table 2 gives a summary of the test sites.

3.1.2 Reference data

Different field data were available for the respective test sites. An overview of the datasets employed in the papers is found in Tables 2 and 3.

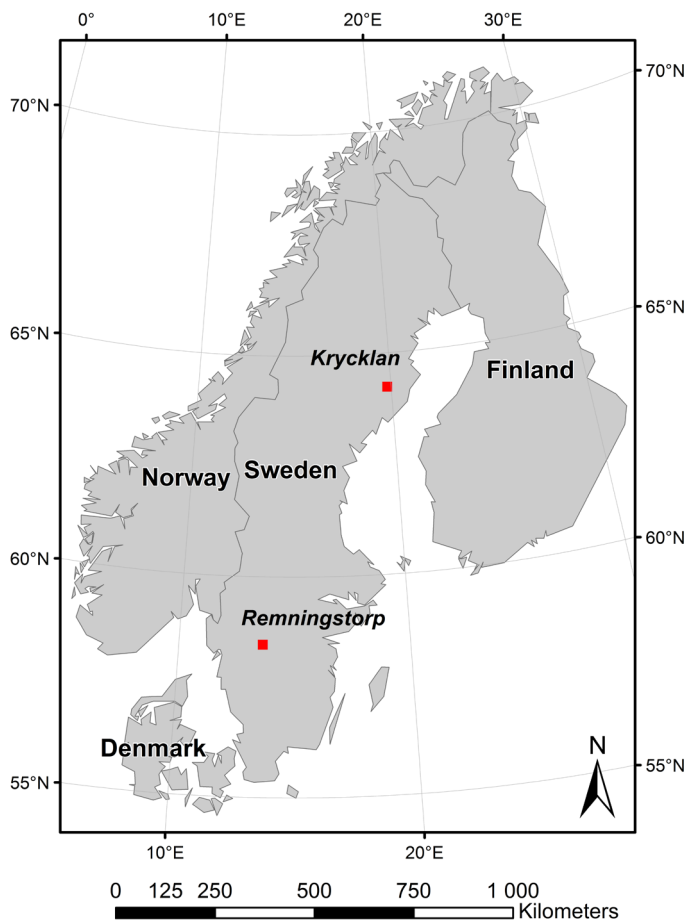


Figure 19. Map over Sweden and the test sites Remningstorp and Krycklan.

Table 2. Summary of the datasets used in the papers.

Dataset	Inventoried	Area	Number of plots/stands	Test site	Paper
D1	2008	452 m ²	110	Krycklan	II
D2	2008	2,4-26,3 ha	31	Krycklan	II, III, V
D3	2008	314 m ²	31	Krycklan	III
D4	2010	314 m ²	212	Remningstorp	I
D5	2010-2011	5,024 m ²	32	Remningstorp	I, II, III, IV, V
D6	2010-2011	314 m ²	32	Remningstorp	III

Table 3. *Summary of statistics for the used datasets.*

Dataset	AGB mean [tons ha ⁻¹]	AGB min [tons ha ⁻¹]	AGB max [tons ha ⁻¹]	H mean [m]	H min [m]	H max [m]
<i>D1</i>	93	12	229	15	11	22
<i>D2</i>	95	23	183	15	8	21
<i>D3</i>	90	5	183	15	6	21
<i>D4</i>	120	1	316	17	4	28
<i>D5</i>	155	55	284	24	16	31
<i>D6</i>	192	72	311	24	16	33

Krycklan

In Krycklan, two datasets, both collected in the period August-October 2008, were available. The first set of data (denoted *D1*) was collected for a previous study described in Hajnsek et al. (2009). Its purpose was to map circular field plots to ALS strips with high pulse density. Therefore, 110 circular plots with 12 m radius were randomly distributed within these strips. All trees with DBH ≥ 4 cm were calipered and for about 5% randomly chosen trees, heights were also measured. The AGB was calculated using functions from Petersson (1999) and the H was computed for all trees using linear regression models.

ALS and field data were used in linear regression models to create reference rasters for the entire test site. Stand-level values of AGB and H could then be extracted from the reference rasters.

In addition, a second field dataset (*D2*) inventoried for the BioSAR 2008 project (Hajnsek et al. 2009) was available, which consisted of 31 densely sampled stands. Each stand was systematically sampled with an average of 10 plots with 10 m radius. The stand estimates were used “as is” while a subset of plots (*D3*) consisting of 1 random plot (10 m radius) from each stand was extracted for plot-level evaluations.

Remningstorp

In Remningstorp two datasets were available. The first (*D4*) was surveyed with a systematic grid of 212 field plots with 10 m radius which were allocated over the estate using 200 m spacing. All trees with a DBH ≥ 4 cm were calipered and for randomly chosen trees, height was also measured after the vegetation season in 2010. ALS and field data were used in linear regression models to create reference rasters for AGB and H that covered the entire test site (Ulander et al. 2010).

The second dataset (*D5*) consisted of 32 circular plots with 40 m radius which were subjectively distributed inside homogenous stands of mature

forest. All trees with a DBH ≥ 4 cm were calipered after the vegetation season in 2010, and about 10% of the trees (randomly selected) were also measured for height. The AGB and H were calculated with the Heureka forestry decision support system (Wikström et al. 2011), using DBH and species as input variables.

The 32 plots were inventoried with positioning of every single tree, which made it possible to extract a subset (*D6*) of circular plots with the innermost 10 m radius and these were used for plot-level analysis.

3.1.3 Satellite data

An overview of all available satellite images used is given in Table 4.

3.1.4 Other data sources

In Paper I orthophotos were used in combination with a 3D relief from an ALS DTM, to find suitable locations for the ground control points (GCPs). These were used as reference points in order to improve the sensor model originally derived from the attached image metadata (e.g., orbit state vectors). The ALS data were acquired from a helicopter in 2010, with the TopEye MkIII system, giving at least 10 points m^{-2} .

In Papers II and III these ALS data were also used for generation of the regression-based reference rasters and height percentiles over Remningstorp. In Krycklan the corresponding reference raster generation and percentile extractions used ALS data from the TopEye MkII system, scanned in 2008, with about 5 points m^{-2} .

In Papers II-V, the DTMs were ALS-based but delivered by the Swedish National Land Survey (Lantmäteriet), which used ALS data with 0.5 points m^{-2} .

3.1.5 Paper I - Stereogrammetry

In Paper I, multispectral data from the SPOT-5 HRG sensor were complemented with 3D data in the form of a CHM from the optical sensors Terra ASTER, SPOT HRS, and ALOS PRISM. The CHMs were created using the software RSG (Remote Sensing Graz; Joanneum Research n.d.) with 10 m pixel size. The multi-spectral data had a pixel size of 10 m while the pixel size of the 2D images from which the CHM was calculated varied. The first sensor evaluated was Terra ASTER with 15 m pixel size. It offered images acquired from nadir and -27.7° along-track look angles. This was too coarse for forestry applications and the sensor was excluded

Table 4. *Satellite images used in this thesis. Acquisition modes: stripmap (SM), spotlight (SL), and high-resolution spotlight (HS).*

Sensor	Acquisition date	Purpose	Resolution [m]	Mode	Paper
SPOT-5 HRG	Jun 4, 2010	Spectral analysis	10	-	I
Terra ASTER	Jul 18, 2008	Stereogrammetry	15	-	I
SPOT-5 HRS	May 10, 2008	Stereogrammetry	10×5	-	I
ALOS PRISM	Jul 7, 2010	Stereogrammetry	2.5	-	I
TerraSAR-X	Oct 11, 2008	Radargrammetry	1.18×6.06	SM	II
TerraSAR-X	Oct 16, 2008	Radargrammetry	1.18×1.38	SL	II
TerraSAR-X	Oct 17, 2008	Radargrammetry	1.18×3.52	SL	II
TerraSAR-X	Aug 22, 2010	Radargrammetry	1.18×1.10	HS	II
TerraSAR-X	Aug 27, 2010	Radargrammetry	1.18×1.10	HS	II
TerraSAR-X	Sep 2, 2010	Radargrammetry	1.18×1.10	HS	II
TerraSAR-X	Sep 7, 2010	Radargrammetry	1.18×1.10	HS	II
TanDEM-X	Jun 4, 2011	Interferometry	1.8×1.10	SM	III, IV, V
TanDEM-X	Jun 17, 2011	Interferometry	1.8×1.10	SM	III, V
TanDEM-X	Jul 17, 2012	Interferometry	2.6×1.10	SM	V
TanDEM-X	Jul 20, 2011	Interferometry	1.8×1.10	SM	V
TanDEM-X	Aug 9, 2011	Interferometry	1.8×1.10	SM	IV, V
TanDEM-X	Aug 11, 2011	Interferometry	1.8×1.10	SM	V
TanDEM-X	Aug 20, 2011	Interferometry	1.8×1.10	SM	IV, V
TanDEM-X	Aug 22, 2011	Interferometry	1.8×1.10	SM	V
TanDEM-X	Jun 1, 2012	Interferometry	2.6×1.10	SM	IV, V
TanDEM-X	Aug 8, 2012	Interferometry	2.6×1.10	SM	V
TanDEM-X	Aug 19, 2012	Interferometry	2.6×1.10	SM	V
TanDEM-X	Aug 28, 2012	Interferometry	2.6×1.10	SM	IV, V
TanDEM-X	Jun 1, 2013	Interferometry	2.6×1.10	SM	V
TanDEM-X	Jun 23, 2013	Interferometry	2.6×1.10	SM	V
TanDEM-X	Jul 2, 2013	Interferometry	2.6×1.10	SM	IV, V
TanDEM-X	Jul 24, 2013	Interferometry	2.6×1.10	SM	IV, V
TanDEM-X	Jul 26, 2013	Interferometry	2.6×1.10	SM	V
TanDEM-X	Aug 4, 2013	Interferometry	2.6×1.10	SM	IV, V

from the analysis. The second sensor evaluated was SPOT-5 HRS, with 10 m pixel size. It had $\pm 20^\circ$ look angle geometry. Finally, ALOS PRISM with 2.5 m pixel size supplied images acquired both from nadir and $\pm 24^\circ$.

3.1.6 Papers II-V - Radargrammetry and interferometry

The images obtained from the TerraSAR-X sensor were acquired in stripmap, spotlight or high-resolution spotlight mode, hence explaining the varying azimuth pixel resolution. The declared resolutions for TerraSAR-X and TanDEM-X are the slant range and azimuth resolutions. The images obtained from TanDEM-X (the bistatic interferometer) were actually pairs of images, where one image originated from the master satellite and the second from the slave (TerraSAR-X/TanDEM-X) in the bistatic setup that was used. The TanDEM-X images were generally acquired in stripmap mode and all SAR images were acquired with incidence angles in the range of 33° to 48°. In Paper II, the HH co-polarization channel was used (because of inconsistency of other polarizations) while Papers III-V used the VV-polarization.

3.2 Methods

Papers I-III have mainly focused on evaluation of CHMs generated with different techniques and the respective performance compared to past satellite data sources and ALS data. In addition, there is a comparison between test sites. Papers IV and V have a stronger focus on development of methods to achieve better estimation of AGB and H.

3.2.1 Data processing

The common denominator for all papers has been to use 3D satellite data in order to create feasible CHMs, from which metrics have been extracted. The processing differs slightly between the papers but for Papers I-III, external dedicated software packages have been utilized, while in Papers IV and V, the processing was performed in Matlab. In Papers I and II, the software RSG was used (Joanneum Research n.d.). The processing for Paper III was performed using the software GAMMA (Gamma n.d.).

The typical processing chain is illustrated in *Figure 20*. The pre-processing consists of co-registration and speckle-filtering, for example. The CHM generation covers the actual 3D reconstruction, which depends on the chosen technique. Post-processing consists of geocoding and sometimes filtering, for example.

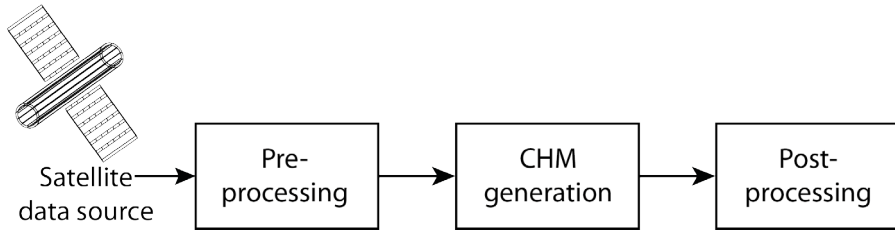


Figure 20. A typical processing chain for all types of satellite data sources used.

3.2.2 Paper I - Stereogrammetry

Paper I describes how well the AGB and H can be estimated at stand-level from spectral satellite data alone, from a CHM generated from optical satellite images, or from a combination of those. The spectral data were acquired with the SPOT-5 HRG sensor, while three different CHMs were evaluated, where the satellite sensors were Terra ASTER, SPOT-5 HRS and ALOS PRISM. Additionally, the sensor producing the most accurate CHM was also evaluated at sub-stand-level.

The generation of the CHM was a time-consuming process that included a lot of manual work. After the raw data import, traditional filters and calibrations were tested. Since the meta-data for these optical data have rather low positional accuracy, careful elaboration of placing GCPs was required in order to rectify the images correctly. At this stage, placing common tie-points in the two images was also carried out by hand (Figure 21). The image matching included many combinations of parameters and the actual processing takes hours and even days for large satellite images on the fast PCs of today. Some post-filtering was tested before the geocoding and the CHMs could then be stored on the form of a 2D raster.

The circular field plots used in this study had a radius of 10 m and in order to estimate areas of similar size, the spectral and CHM rasters were resampled from 10 m to 17.5 m pixels. Different metrics were extracted from the spectral and CHM rasters and fitted parameters were found through linear regression. These were evaluated using the leave-one-out cross-validation method (further described in Section 3.2.8). The sub-stand level models were trained on the complete set of field plots (*D4*) and thereafter evaluated on the other dataset of sub-stands (*D5*).

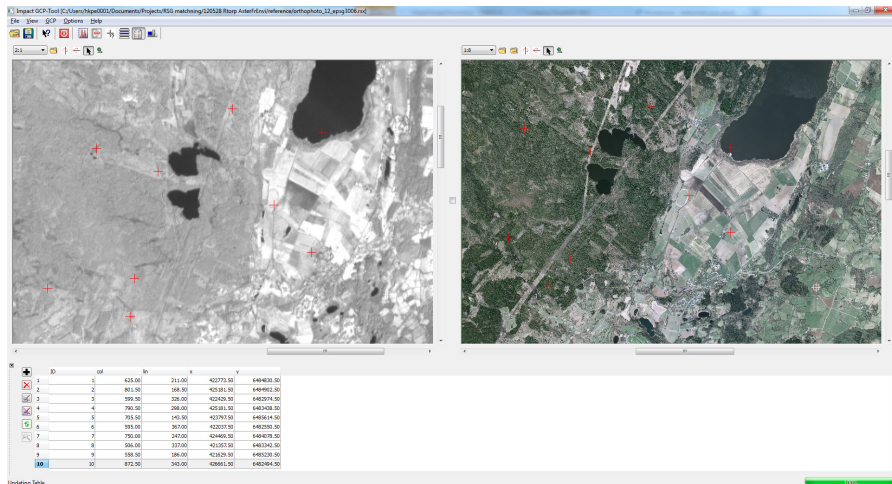


Figure 21. An example of how GCPs were manually placed in the satellite image (left) and in the orthophoto (right).

3.2.3 Paper II - Radargrammetry

In Paper II, the radargrammetric processing technique was applied to TerraSAR-X imagery in order to generate a high-precision CHM. The effects of different incidence angles, image resolutions, tree species and terrain topography were considered.

The processing chain was to a large extent similar to the one in Paper I. The meta-data for both the satellite positioning and the ground images were sufficiently accurate, and the manual time-consuming steps used in Paper I could be avoided. The CHM generated was then trained with linear regression analysis and evaluated with the leave-one-out cross-validation method at stand-level ($D1$, $D2$, and $D5$).

3.2.4 Paper III - Interferometry

Paper III describes how TanDEM-X data can be used in InSAR processing to generate accurate CHMs and coherence-maps at the two test sites Krycklan and Remningstorp. By using the SPC and the coherence, the AGB and H were estimated at plot- and stand-level, and moreover compared to both *in situ* data and the corresponding ALS estimations.

As input the TanDEM-X image-pairs were processed according to a traditional InSAR processing chain with the GAMMA software (Gamma n.d.). The obtained outputs were an interferometric height map and a coherence map, both in ground range geometry.

The images were delivered by DLR and before delivery some pre-processing was already carried out (Duque et al. 2012). The two images were acquired in a bistatic configuration; hence the images were focused at their respective zero-Doppler time and then the common spectrum was filtered to improve the interferometric phase quality. This implied a minor resolution loss (as the bandwidth decreased, recall Section 1.4.1) of about 3-5%. Finally, the images were accurately co-registered with sub-pixel accuracy. The co-registered slant range single look complex (CoSSC) images were delivered and could be imported in the GAMMA software.

The processing was then carried out in slant-range geometry and as the final product was used in ground-range geometry, a lookup-table (LUT) for the transformation between the geometries was generated with the ALS based DTM from Lantmäteriet as ground-range truth. The complex radar interferogram was then generated ($\text{image}_1 \times \text{image}_2^*$, recall Eq. 13) and with the accurate ALS DTM as input, the ground phase could be calculated over the entire scene making a complete terrain phase removal possible. The remaining phase was then unwrapped, i.e., the phase describing the CHM was shifted to make the zero-phase correspond to zero-height, and converted to the interferometric height. Also the coherence map was extracted from the complex interferogram. Both the interferometric height map and coherence map were finally converted to ground-range geometry through the LUT earlier established. Plot- and stand-mean values were then extracted from the generated maps (therefore being non-coherent values) and similar to the other studies, using regression analysis, the parameters were determined and the models were evaluated with the leave-one-out cross-validation method for the datasets *D2*, *D3*, *D5* and *D6*.

For comparison, ALS height rasters for different percentiles and the VR were generated with the Lastools software (Isenburg n.d.). These rasters were correspondingly modeled and evaluated.

3.2.5 Paper IV – Two-level model inversion of tree height and canopy density

Paper IV describes how an interferometric two-level model (TLM) can be inverted in order to estimate H and forest canopy density. The TLM can be seen as a simplified version of the physical model IWCM presented in Section 1.6.5. Several differences between the models exist, although many similarities remain.

The TLM models the vegetation as a homogenous medium consisting of random scatterers randomly oriented as a “water cloud” above ground, just as IWCM. The TLM includes also the gaps appearing in-between the trees,

which contains important information about the forest density. Unlike the IWCM, TLM does not require polarimetric data or multi-temporal data. It describes exact formulas for the level separation distance Δh , area-weighted backscatter ratio μ and the uncorrected area-fill factor η_0 .

$$\eta_0 = \frac{1}{1 + \mu} \quad (30)$$

It also replaces the integrals with sums of two discrete scattering levels. All this makes TLM simpler than both IWCM and RVoG, where RVoG requires complex methods for procedures such as the extraction of coherence regions.

The IWCM can in its simplest form be seen as a model with five unknown parameters. In its full formulation which was originally developed for stem volume estimation from repeat-pass ERS-1/2 interferometry (Askne et al. 2003), the IWCM included additional empirical functions and temporal decorrelation modeling. In RVoG the gaps are not modeled and only one consistent “random volume” is modeled above ground, leading to the number of parameters decreasing to four. The cost for this decrease of parameters can be rather crucial, as the lack of the parameter describing the gaps makes description of forest density difficult.

Several solutions to solve for all four unknown parameters in RVoG were presented in Section 1.6.6, but the most common solution has been to use several polarizations. The desired combination of these are not always available and by replacing the homogenous medium in the RVoG model with a closed layer of infinite extinction, located at the SPC, but also modeling the gaps like the IWCM model, where the gaps get their closed layers located at the ground-level, the numbers of parameters are decreased to three in the TLM. One of these parameters is the ground phase, which is often known from accurate ALS data. The remaining two parameters can therefore be computed from just one single ground-corrected InSAR complex correlation coefficient $\tilde{\gamma}$ (Eq. (14)). These carry information about both forest height and forest density, in a much simpler manner than IWCM and RVoG.

The InSAR processing that takes place, in order to solve for the unknown parameters ground-to-vegetation ratio μ and Δh , is similar to the one presented in Section 3.2.4, but was carried out entirely in Matlab. The process can be summarized as 1) geo-referencing and DTM interpolation, 2) DTM interferogram computation, 3) TanDEM-X interferogram flattening, and 4) inversion of parameters. Important differences to mention

are first that no unwrapping was applied, driven by the fact that the *HOA* for all processed images is larger than all the known tree heights occurring at the used test sites. Therefore no ambiguities due to this could occur. Moreover, the inversion is taking place in the complex domain, meaning the images are still in the slant-range geometry, which allows for coherent extraction of the sought parameters.

3.2.6 Paper V – Two-level model based inversion of AGB

In Paper V, the TLM was used in a power function for estimation of AGB at the two test sites Krycklan and Remningstorp. By using Δh and η_0 from the TLM, the AGB is described as

$$AGB = K \cdot \Delta h^\alpha \cdot \eta_0^\beta \quad (31)$$

and the unknown parameters K , α and β are found from regression analysis. The models are evaluated on the datasets *D2* and *D5*, which are the densely sampled stands in Krycklan and the 32 large plots in Remningstorp. In total 18 image pairs were inspected.

An important difference to other studies was that a direct parameter η_0 describing the forest density was used for the AGB estimations. Regression analysis was used to find the most suitable overall values for K , α and β , in the estimations of AGB and these simpler models were also discussed in comparison to the results obtained for single-scene fitted results.

3.2.7 Model analysis

It has been mentioned throughout the text, that model parameters were estimated from different analyses. This has sometimes been given the expression “training” the model. The expression “training data” is for the dataset containing data on the parameter to be estimated and the corresponding image data value. For example, the spectral value of a pixel in a digital image is mapped to a forest variable measured in field. Simplified, this means that the pixel value (say 97) has been “trained” to correspond to a certain value of the measured field variable (e.g., the tree height 12 m). This is then used to extrapolate this knowledge to the entire image, claiming that all pixels with value 97 can be expected to have a tree height of 12 m.

A different approach is the use of mathematical models to theoretically describe different forest properties, such as the tree height change. One of the most common models relates AGB or stem volume to DBH through the allometric equation

$$y = a \cdot x^c \quad (32)$$

$$\ln(y) = \ln(a) + c \cdot \ln(x)$$

where the response variable y typically represents the AGB and x the DBH. The exponent c is a measure of how much the biomass increases with increased diameter and is dependent on several factors such as species and local site conditions.

Throughout this thesis, multiple linear regression analysis has commonly been used for training the models, which in this sense means finding the parameters that minimize the distance between the model and the data, more specifically parameters that minimize the sum of the squared residuals for the model applied to a specific dataset. Linear regression is powerful and if correctly used can also describe non-linear relationships, either by transforming the response variable (log-transformations are frequently used) or by transforming the explanatory variables (e.g., squaring the height to model the AGB as $AGB=H^2$). A typical linear regression model can be described as

$$y = f(\mathbf{x}|\boldsymbol{\beta}) + \epsilon = \beta_0 + \beta_1x_1 + \dots + \beta_nx_n + \epsilon \quad (33)$$

where y is the response variable, $\mathbf{x} = (x_1, \dots, x_n)$ are the explanatory variables, $\boldsymbol{\beta} = (\beta_0, \dots, \beta_n)$ are the regression coefficients and ϵ is a random error. The linear regression model and the validity of accompanying t -tests rests on four assumptions: 1) linearity and additivity of the relationship between dependent and independent variables; 2) statistical independence of the errors; 3) constant variance of the errors; and, 4) the errors are normally distributed. In addition to these assumptions, the appropriate explanatory variables have to be included in the model for valid results. Bias or uncorrelated predictions might otherwise be the result and for an efficient model selection it is normally helpful to visualize the data with graphical plots.

3.2.8 Accuracy assessment

The main measure for determining the estimation error used in this thesis is root mean square error (RMSE), which is the square root of the average squared errors.

To calculate the RMSE between the model and the prediction, independent model training data and validation datasets can be used (partly used in Paper I). Another option is to use leave-one-out cross-validation

which was used in the studies I-III, where the model is trained (i.e., the parameters are determined by least-squares) with all but one plot/stand in the entire dataset. The difference between the predicted left-out plot or stand and the model can then be determined. This is done for all plots or stands, one at a time, to compute the full set of residuals, which can be used to calculate the RMSE.

When the leave-one-out method is used, there is a risk for overfitting, meaning that the model is describing the noise rather than the underlying relationship. This can be the case especially when the number of samples is small (e.g., in Paper II this is mentioned for the stand evaluation on 20 stands). This overfitting can be computed as the square root of the ratio between the predicted sum of squares of residuals and the ordinary sum of squares of residuals (Weisberg 1985) denoted q . It takes the value of a positive number, ≥ 1 , where 1 means no overfitting has occurred, whereas larger values means there is increased overfitting. Typically values < 1.10 can be considered as not particularly overfitted.

In Papers I-III and V, the measure R_{adj}^2 was used, which stands for the adjusted coefficient of determination, and takes a value between 0 and 1. It indicates how well data points fit a statistical model and R^2 was defined by (Kvålseth 1985) as

$$R^2 = 1 - \frac{\sum(y_i - \hat{y}_i)^2}{\sum(y_i - \bar{y})^2} \quad (34)$$

where y_i is the variable to be estimated, \hat{y}_i are estimates of y_i , and \bar{y} is the mean value of y . An interpretation of R^2 is that it indicates how large a part of the variation in the response variable is explained by the predictor variables (Rawlings et al. 1998). The “adjusted” is an attempt to account for the phenomenon of the R^2 automatically increasing when extra explanatory variables are added to the model.

$$R_{adj}^2 = 1 - (1 - R^2) \frac{n - 1}{n - p - 1} \quad (35)$$

where p is the total number of regression coefficients in the linear model (not counting the constant term), and n is the sample size.



4 Results and discussion

All papers have fundamentally examined the same objectives of using 3D satellite data to improve forest variable estimation, but with slightly different reference data and remote sensing data. Despite the existing local differences, the RMSE values computed still possess a rough but most likely accurate indication of the potential with each respective technique and approach. All best-case RMSEs are listed in Tables 5 and 6. Due to the importance of accurate height information captured using each respective technique, examples of different CHMs are shown from a region in Remningstorp in *Figures 22-24*.

Table 5. Overview of the AGB accuracy obtained with the different techniques at stand-level.

Technique	RMSE (tons ha ⁻¹)	RMSE (%)	Paper	Test site
Stereogrammetry	31.8	26.2	I	Remningstorp
Radargrammetry	24.9	22.9	II	Remningstorp
Interferometry	22.2	14.4	III	Remningstorp
Interferometry	16.9	11.8	V	Remningstorp

Table 6. Overview of the H accuracy obtained with the different techniques at stand-level.

Technique	RMSE (m)	RMSE (%)	Paper	Test site
Stereogrammetry	2.4	16.1	I	Remningstorp
Radargrammetry	1.2	7.7	II	Krycklan
Interferometry	1.0	4.1	III	Remningstorp
Interferometry	1.0	5.6	IV	Remningstorp

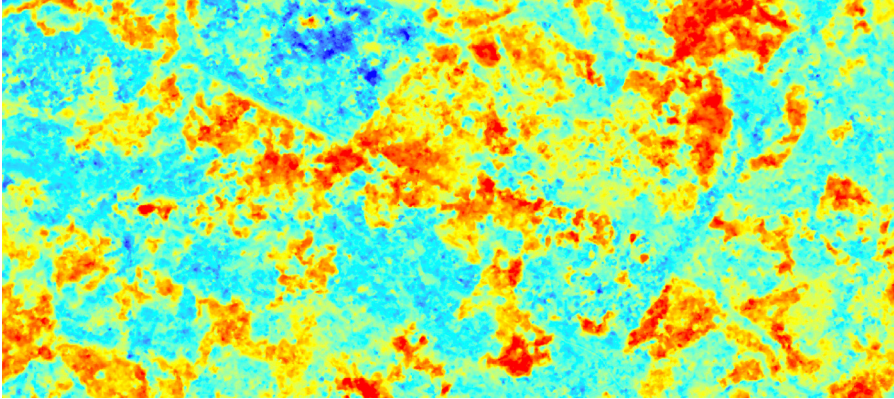


Figure 22. Remningstorp CHM from ALOS PRISM data created with stereogrammetry.

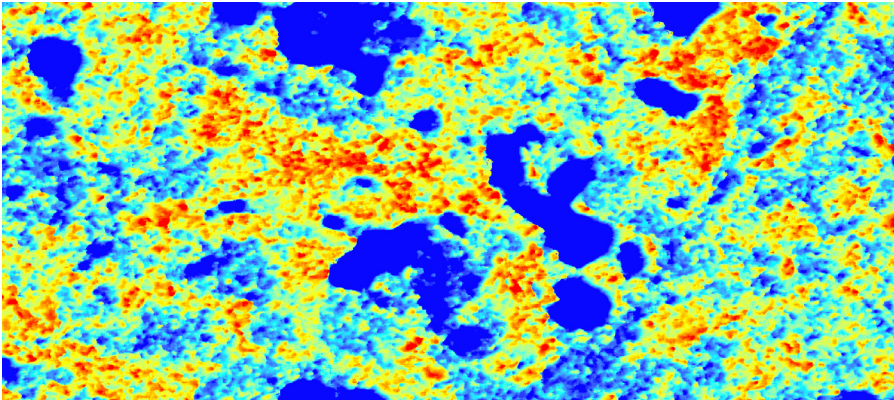


Figure 23. Remningstorp CHM from TerraSAR-X data created with radargrammetry. The large blue blobs are mismatched regions with no height information available.

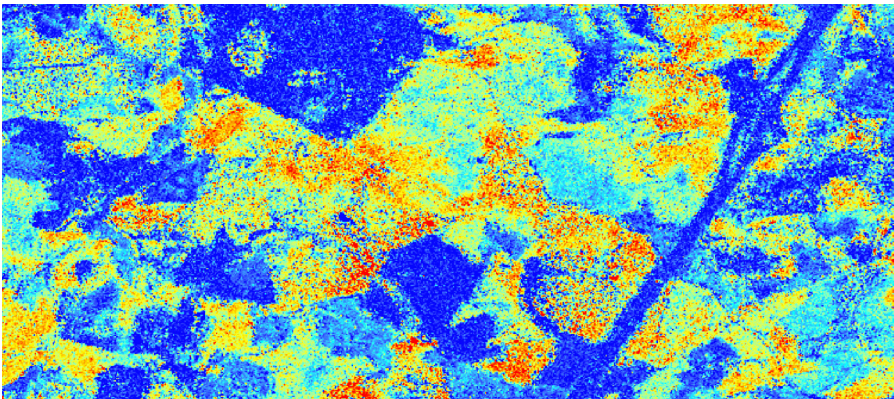


Figure 24. Remningstorp CHM from TanDEM-X data created with interferometry.

4.1 Stereogrammetry

In Paper I, it was found that optical satellite images could be used in stereogrammetric modeling for estimation of AGB and H. By using the ALOS PRISM sensor, 26.2% and 16.4% RMSE was attained at stand-level, respectively. When the spectral information from optical satellite images (SPOT-5 HRG) were used (a traditional approach), the corresponding accuracies were 32.9% and 16.1%. The interesting evaluation was the fusion of these, which showed that they bear partially independent information about the forest and hence the non-overlapping contributions added up to improved total estimation accuracies being 22.4% and 12.9% at stand-level for AGB and H, respectively. These values are on the same order as manual measures attained *in situ*, but with the advantage that they can be carried out over much larger areas with significantly less effort.

The ALOS PRISM sensor was also evaluated on a different dataset (*D5*), which corresponded to small stands (0.5 ha large) and these were also used as stands in Paper III. This evaluation gave lower RMSEs than with dataset *D4*, despite the average smaller evaluation units. The RMSE decreased from 22.0% to 20.6% for the AGB estimations and the H estimations decreased from 13.6% to 10.5% RMSE. The surprising results on a relative scale might be a consequence of different types of forests. When examining the absolute RMSEs, it can be seen that the RMSE for AGB estimation even increased while the H was more or less constant. After becoming more familiar with the datasets, it could be concluded that dataset *D5* contained only mature forest, which caused an upward displacement of the average AGB and H values. This in turn made the relative RMSEs deceptively look slightly better with dataset *D5* than with *D4*. It can be a combination of several other reasons too (as stated in the published paper), such as that dataset *D4* was used in combination with ALS data to create the reference dataset, while *D5* represented the pure field measurements only.

There is obviously an advantage to adding 3D data when estimations of this kind are to be achieved, however, the choice of sensors must be considered. This conclusion became clear as the significant contribution of stereogrammetry did not appear until the ALOS PRISM sensor with 2.5 m ground sampling distance (GSD) was used. The height information from the SPOT-5 HRS sensor did not contribute significantly; SPOT-5 HRS's 10 m GSD might be part of the problem. The look angles probably also played a role, with ALOS PRISM possessing a 48° intersection angle, while the sensor delivering the worst data, Terra ASTER, had both the lowest intersection angle (28°) and the largest pixel size (15 m GSD), while

SPOT-5 HRS had a 40° intersection angle. High spatial resolution (finer GSD) has a large drawback though, that it usually also decreases the swath width, which is one of the main advantages of satellite imagery.

No convincing saturation effects could be detected, but from the Figure 4 in Paper I, it can be suspected that the AGB estimation using the combination of SPOT-5 HRG and SPOT-5 HRS as data sources has a tendency to decrease its linearity, when the biomass reaches about 200 tons ha⁻¹. This cannot be seen for the combination of SPOT-5 HRG together with ALOS PRISM. Because of ALOS PRISM's finer resolution, it is more likely to actually find openings between trees and in the canopy, to reflect a more correct tree height in conifer forest.

The use of optical satellite sensors is justified, as they offer easy-to-interpret imagery with decent performance. However, as optical sensors only deliver images during daylight cloud-free passes, their possibility of supplying frequent imagery is limited. In the boreal zone, the number of annual cloud-free days with enough daylight is restricted and at southern latitudes problems with clouds becomes considerable.

4.2 Radargrammetry

When TerraSAR-X images were used stereogrammetrically instead of optical images, the H estimation could be achieved with 7.7% RMSE at stand-level (Table 6). The AGB estimations were of similar accuracy as with optical data but showed certain robustness, being less dependent of the resolution (and possibly intersection angles) than optical data seemed to be. A rather limited set of intersection angles were tested (6.9° - 15.3°), but the accuracies were not proportionally correlated to these. This agrees with Raggam et al. (1997), Sylvander et al. (1997), and Toutin (1999), who also concluded that larger intersection angles did not necessarily increase the accuracy.

It was also found that among the tested tree species (pine, spruce and deciduous), the estimation for spruce could be achieved with the highest accuracy. Overall, conifer trees appeared similar while deciduous trees performed differently perhaps due the season (leaf-on/leaf-off) as well as that their branch and leaf distribution differs distinctly from that of conifers.

As soon as SAR images were used instead of optical images, the amount of images available increased rapidly, independent of weather conditions. On the other hand, the used SAR satellite tends to stay within certain orbits, which are set beforehand, and therefore it was difficult to obtain suitable

radar images acquired over the same region from different orbits, and with a temporal restriction of 1-2 weeks.

Radargrammetry appeared to be sensitive to ground topography and to the changes of backscattering in regions with hillsides. This sensitivity could not be compared to the optical stereogrammetric case, as only the flatter Remningstorp test site was used in the optical study. It would be important to know, however, in order to conclude whether the topographic effects depend on the stereogrammetric technique or the type of data source. Before radargrammetry can become an efficient operational method, at a minimum, correct masking methods for topographically influenced regions have to be developed, and in the best-case, correction methods should be available to avoid erroneous models. In Toutin (2002) the DEM accuracy against ground slopes was investigated and the correlation between slope and accuracy was almost linear, with the larger errors in the steepest slopes. Attempts were carried out in Paper II to justify this claim also for forest canopies occurring on slopes, but no linear correlation could be concluded. This might still be the case and should be further investigated, but in Paper II there were too few stands on the steeper slopes to obtain reliable results.

In Vastaranta, Niemi, et al. (2014), a non-parametric method was used and it was found that the estimations of basal area, stem volume and AGB based on radargrammetry were overestimated, probably because the small openings in the canopy were too small to be detected with the current technique. Since linear regression analysis was used in the present paper, it is unlikely that there would be bias given that the explanatory variables were correctly chosen. By training the model at one test site and evaluating it on the other, a bias could possibly be found.

The penetration depth was neither computed in percentage of the canopy height nor as an absolute penetration in meters. This question would be of importance especially when model training appears in a different region than where the models are applied. Presumed that penetration appears, young forest with a mean tree height of a couple of meters could appear either with zero heights or with only slightly lower (in percentage) heights than the actual tree heights.

Radargrammetry has, to the current knowledge of the author, not yet been examined in frozen conditions. The reason for the absence of this in the literature and also in this thesis, is the deficit of images. This could potentially improve the forest parameter estimation accuracy of radargrammetry, which inherently is dependent on similar images despite

the temporal baseline. During frozen conditions this stability could likely increase.

Limited experience exists for the influence of the forest density when radargrammetry is used. With improved image resolution, single trees may soon be possible to delineate but until then, the DSM between single trees is likely assigned rough values somewhere in-between the actual canopy height and the ground, when sparser forest is analyzed. On the other hand, dense forest does not facilitate a correct analysis of the AGB in particular, as lower level objects become hidden. In extension to this subject, the effect of leaf-on conditions needs further examination in comparison to leaf-off conditions during the winter. It would be of great interest if a physical relationship which also includes the wavelength dependency could be derived. No saturation could be identified from any of the test sites and this is an important and strong advantage of radargrammetry compared to optical stereogrammetry.

4.3 Interferometry

When all data in the SAR imagery were utilized, it was shown to be the most accurate method tested in this thesis. The height information obtained from the phase was important and alone contributed more than any earlier source of information. When the in-coherently accumulated coherence was added to the AGB and H models, the degree of how well the variations in the models could be explained increased by as much as another 15%.

In Paper III, the TanDEM-X InSAR based models performed on the same order as ALS estimations, with the RMSEs being 14-17% for AGB and 4-8% for H at stand-level at the two test sites. It was also shown, that tree height estimations could be achieved with better accuracy from InSAR data than from ALS data, when evaluated on the same material. It was further found, that the interferometric height seemed linearly correlated to the H.

When the inversion models originating from IWCM and RVoG took advantage of the inherit power of InSAR it was found that accurate AGB estimations could also be attained on test sites without using training data (Paper V). The accuracies for estimations on the same test site were similar to those found in Paper III but with one image pair resulting in excellent AGB accuracy with an RMSE of 11.8%.

In Paper IV it was shown that the TLM could explain the SPC as a biased estimate of ALS percentile 95 (p95) but it was also compared to p50, resulting in an RMSE of 1.0 m, corresponding to 5.6%. As this was

relative ALS heights, the mean height was lower than the H used in Papers I-III, and the relative accuracy appears larger. In Paper III the TanDEM-X data were also used to estimate ALS p99 and the VR, with an absolute RMSE of 0.6-0.7 m for p99, corresponding to 2.7%-4.8%. In Paper IV, it was shown how the TLM inversion could explain the VR, which is an important forest density parameter, with about 9%-11% RMSE.

The TLM brought some important insights, for example, when scattering took place mainly in either one of the two levels, the interferometric height became fairly independent of *HOA*. When both levels were equally well represented as SPCs, a significant interference effect was observed for low HOAs that could cause either negative interferometric heights or heights exceeding the actual tree heights. This interference effect became weaker for $HOA > 2\Delta h$. The TLM worked well also for clear cut and commercial thinned forest, even though the Δh sometimes became biased. This is likely a result of other decorrelation effects caused by, for example, SNR decorrelation, system decorrelation or residuals in the volume decorrelation, which the TLM did not handle.

No conclusions have been drawn in the presented studies about how humidity and weather conditions influence the interferometric technique, but in this thesis work no tendencies have been seen regarding the humidity having any stronger influences on the CHM quality. A difference has been noticed between frozen/unfrozen conditions. Estimations based on images acquired in frozen conditions seem to generate a lower RMSE (18.6%) compared to unfrozen (23.1%). On the other hand, the H could be estimated with 5% RMSE from the summer acquisition while estimations based on the winter acquisition gave 7% RMSE (Ulander et al. 2013).

None of the interferometric models have shown saturations for higher biomasses and the X-band signal seems to penetrate deeper into the canopy than one would expect. It needs more investigation in denser and taller forest though, such as tropical and rain forest.

In comparison to the stereogrammetric and radargrammetric methods, interferometry appeared much more robust and delivered much higher accuracy. The TanDEM-X satellite flight formation offers superior chances to obtain numerous acquisitions of high quality at every pass, 24/7, without weather concerns or worries about enough daylight. Moreover, the interferometric processing technique did not seem to be influenced by the topography. This appeared to be the case at least as long as the decorrelation volume above ground was present. The reason for interferometry being less sensitive to the influence of topography might be subject for a study itself. The difference of radargrammetry being

dependent only on the amplitude and rather large intersection angles creates different geometric setups compared to InSAR, with small intersection angles and the phase being a crucial information carrier.

The resulting tree height and forest density information attainable from interferometry is now approaching or even surpassing the reference data in quality. In order to further improve and validate the interferometric methods, reference data of higher quality might be crucial.

4.4 Concluding remarks

Remote sensing is a powerful technique that can be used to combine different types of data sources, in order to efficiently gain immediate knowledge over large regions. The development shows no signs of becoming stagnant and many different remote sensing techniques serve a variety of useful purposes. Over the last decade, ALS has been the superior technique in forest remote sensing, primarily because it has been shown that the accurate height measurements which can be derived from ALS are important to improved forest parameter estimations. ALS has also made accurate, long-lasting DTMs available in many countries. In this thesis, the main focus has lied on how different satellite-borne sensors can be used in order to gain information especially about the third dimension, height, in order to improve estimates of forest variables, primarily above-ground biomass and tree height. This is important in order to overcome for example signal saturation effects seen in estimates based on 2D images. Different processing techniques which are partly interconnected to the sensor have been implemented and the results were evaluated in different conditions. The two test sites, Krycklan and Remningstorp in northern and southern Sweden, respectively, have served as evaluation forests with varying conditions within boreal forests.

The satellite mission TanDEM-X has delivered imagery with qualities approaching new levels over the last decade with excellent resolution. With its configuration it has also made new applications possible in pace with the constantly improved accessibility. The three processing techniques stereogrammetry, radargrammetry and interferometry have been compared, where stereogrammetry was the only technique that used optical images. The interferometric technique seems to deliver the most accurate CHMs, which were used to estimate the forest variables AGB and H. It was shown that estimations could be reached with accuracies which are in line with other well-known techniques such as ALS, which the last decade regularly has been used as reference data. The situation has become very interesting

in the sense that, especially for biomass estimations, there is likely better remotely sensed data than ground truth data to use in evaluation.

Both empirical and semi-empirical models have been evaluated and they perform on the same order for both AGB and H estimations, which is an important result, as the need of expensive *a priori* field data decreases.

We are facing a bright future for remote sensing and satellite-borne systems have an evident position in this future.

4.5 Future work

Despite the finished studies, more work can of course always be done. In relation to the respective techniques in Sections 4.1-4.3, different open questions were discussed. First of all, a better understanding of these ideas would be important. The potential of the techniques with respect to the currently available imagery is rather well analyzed and it is more a question of solving the special cases and limitations of the different techniques, which are hindering them from quickly becoming potent commercial products. One example of this would be the topographic sensitivity for radargrammetric based estimations. It was shown in Solberg et al. (2015) that two radargrammetric image pairs acquired from different orbit directions could be used to estimate AGB and H as well as InSAR based estimations. The problem with topography for radargrammetry in regions with hillier terrain still needs to be solved and as an extension to Toutin (2002), it would be an interesting study to investigate the influence of trees on bare ground, at different slopes. Both simulations and validation of these on real data would greatly expand the current knowledge and usage of radargrammetry.

As further steps, new questions have arisen in relation to the work presented here on this theme over the last couple of years. There are so many more things to discover, both for myself but of course also for the scientific community. Most of the studies I have encountered are concerned about having some knowledge in advance about the local forest conditions in order to say something about the surrounding forest. This *a priori* requirement is an important drawback of how remote sensing currently can be used. Deriving confident conclusions from satellite data with limited local knowledge is one of the biggest challenges of today. If this problem could be solved, interesting online services could be available in the future, for example, almost real-time estimations of AGB and H supporting forest management recommendations at stand-level automatically. This would also be an excellent tool, for example, for the entire chain supplying the

paper industries and saw mills, giving the “just-in-time” production strategy a new meaning in the base industry as well.

There is also a tendency towards the occurrence of more storms and wind thrown trees as a result, caused by global warming. This will lead to warmer winters with more heavy snow weighing on the trees in combination with strong wind, which will likely cause forest owners extensive costs as the forest has to be cleared away. Several severe storms have hit Sweden just in the last decade and it would be of large value to develop efficient tools for locating affected regions as well as being able to accurately estimate forest stem volume and where it is located. Closely related to this theme, Sweden experienced an extensive forest fire in the summer of 2014. Future remote sensing based applications could possibly help to detect fires at an earlier stage, and thus limit the damages.

Time will tell.

References

- Ager, T.P. & Bresnahan, P.C., 2009. Geometric precision in space radar imaging: results from TerraSAR-X. In *ASPRS 2009 Annual Conference*. March 9-13, 2009, Baltimore, Maryland, USA, p. 8.
- Anon, 2003. IEEE Standard Letter Designations for Radar-Frequency Bands. *IEEE Std 521-2002 (Revision of IEEE Std 521-1984)*, pp.1–3.
- Arnaubec, A. et al., 2014. Compact PolInSAR and Homogeneous Random Volume Over Ground Model. *IEEE Transactions on Geoscience and Remote Sensing*, 52(3), pp.1879–1891.
- Askne, J. et al., 2013. Model-based biomass estimation of a hemi-boreal forest from multitemporal TanDEM-X acquisitions. *Remote Sensing*, 5(11), pp.5574–5597.
- Askne, J. et al., 2003. Multitemporal repeat-pass SAR interferometry of boreal forests. *IEEE Transactions on Geoscience and Remote Sensing*, 41(7), pp.1540–1550.
- Askne, J. et al., 1995. Retrieval of forest parameters using intensity and repeat-pass interferometric SAR information. In *Proceedings of Retrieval of Bio- and Geophysical Parameters from SAR Data for Land Applications*. 10-13 October, 1995, Toulouse, pp. 119–129.
- Askne, J., Danmert, P.B.G. & Smith, G., 1999. Understanding InSAR Coherence of Boreal Forests. In *IGARSS 1999*. 28 June - 2 July, 1999, Hamburg, Germany, pp. 2111–2114.

- Askne, J. & Smith, G., 1996. Forest INSAR decorrelation and classification properties. In *FRINGE 96*. 30 Sep-2 Oct, 1996, Zurich, pp. 95–103.
- Askne, J.I.H. et al., 1997. C-band repeat-pass interferometric SAR observations of the forest. *IEEE Transactions on Geoscience and Remote Sensing*, 35(1), pp.25–35.
- Attema, E.P. & Ulaby, F.T., 1978. Vegetation modeled as a water cloud. *Radio Science*, 13(2), pp.357–364.
- Balzter, H. et al., 2007. Observations of forest stand top height and mean height from interferometric SAR and LiDAR over a conifer plantation at Thetford Forest, UK. *International Journal of Remote Sensing*, 28(6), pp.1173–1197.
- Bamler, R. & Hartl, P., 1998. Synthetic aperture radar interferometry. *Inverse Problems*, 14(4), p.R1.
- Bergström, H., Melin, H. & Nicolausson, A., 2009. *Höjddata – en förutsättning för klimatanpassning*, Gävle, Sweden: Swedish National Land Survey.
- Born, M. & Wolf, E., 1980. *Principles of Optics 6th ed* 6th ed., Cambridge, UK: Cambridge University Press.
- Bresnahan, P.C., 2011. *Geolocation Accuracy Re-Evaluation of Cosmo-Skymed Spotlight and Stripmap Imaging Mode Products*, Boulder, CO, USA.
- Brovkin, V. et al., 2012. Plant-driven variation in decomposition rates improves projections of global litter stock distribution. *Biogeosciences*, 9(1), pp.565–576.
- Büyüksalih, G. & Jacobsen, K., 2007. Comparison of DEM generation by very high resolution optical satellites. *New Developments and Challenges in Remote Sensing*, pp.627–637.
- Caicoya, A.T. et al., 2012. Boreal forest biomass classification with TanDEM-X. In *IEEE International Geoscience and Remote Sensing Symposium*. Munich, Germany, 22-27 July, 2012, pp. 10–13.

- Canadell, J.G. et al., 2007. Contributions to accelerating atmospheric CO₂ growth from economic activity, carbon intensity, and efficiency of natural sinks. *Proceedings of the National Academy of Sciences of the United States of America*, 104(47), pp.18866–70.
- Chaisson, E. & McMillan, S., 2003. *A Beginner's Guide to the Universe 4 ed* 4th ed., Pearson Education.
- Cloude, S.R. & Papathanassiou, K.P., 2003. Three-stage inversion process for polarimetric SAR interferometry. *Radar Sonar Navigation*, 150(3), pp.125–134.
- Cornwell, W.K. et al., 2008. Plant species traits are the predominant control on litter decomposition rates within biomes worldwide. *Ecology letters*, 11(10), pp.1065–71.
- Dammert, P.B.G., 1999. *Spaceborne SAR Interferometry: Theory and Applications*. Chalmers University of Technology.
- Ducey, M.J., 2009. Sampling trees with probability nearly proportional to biomass. *Forest Ecology and Management*, 258(9), pp.2110–2116.
- Duque, S. et al., 2012. *TanDEM-X Payload Ground Segment: CoSSC Generation and Interferometric Considerations*, DLR.
- Dutra, L. & Elmiro, M., 2002. Assessment of digital elevation models obtained in Brazilian Amazon based on P and X band airborne interferometric data. In *IGARSS 2002*. 24-28 Jun, Toronto, Canada, pp. 3617–3619.
- Ferretti, A. et al., 2007. *InSAR Principles-Guidelines for SAR Interferometry Processing and Interpretation* TM-19th ed. K. Fletcher, ed., Noordwijk, Netherlands: ESA Publications.
- Floyd M. Henderson (Editor), A.J.L. (Editor), 1998. *Manual of Remote Sensing, Volume 2, Principles and Applications of Imaging Radar, 3rd Edition*, John Wiley & Sons.
- Fransson, J.E.S. & Israelsson, H., 1999. Estimation of stem volume in boreal forests using ERS-1 C- and JERS-1 L-band SAR data. *International Journal of Remote Sensing*, 20(1), pp.123–137.

- Fritz, T., Breit, H. & Eineder, M., 2008. TerraSAR-X Products – Tips and Tricks. In *3rd TerraSAR-X Workshop*. November 25-26, 2008. Oberpfaffenhofen, Germany, p. 61.
- Fullerton, K., Leberl, F. & Marque, R., 1986. Opposite-Side SAR Image Processing for Stereo Viewing. *Photogrammetric Engineering and Remote Sensing*, 52(9), pp.1487–1498.
- Gamma, Gamma Remote Sensing Consulting AG Software. Available at: <http://www.gamma-rs.ch/>.
- Garestier, F., Dubois-fernandez, P.C. & Papathanassiou, K.P., 2008. Pine Forest Height Inversion Using Single-pass X-band Polinsar Data. *IEEE Transactions on Geoscience and Remote Sensing*, 46(1), pp.59–68.
- Gatelli, F. et al., 1994. The wavenumber shift in SAR interferometry. *IEEE Transactions on Geoscience and Remote Sensing*, 32(4), pp.855–865.
- Goldstein, R.M., Engelhardt, B.K. & Frolich, R.M., 1993. Satellite radar interferometry for monitoring ice sheet motion: application to an antarctic ice stream. *Science*, 262(5139), pp.1525–1530.
- Gracie, G. et al., 1970. *Stereo Radar Analysis*, Defense Technical Information Center.
- Hagberg, J.O., Ulander, L.M.H. & Askne, J., 1995. Repeat-pass SAR interferometry over forested terrain. *IEEE Transactions on Geoscience and Remote Sensing*, 33(2), pp.331–340.
- Hajnsek, I. et al., 2008. *BioSAR 2007. Technical assistance for the development of airborne SAR and geophysical measurements during the BioSAR 2007 experiment: Final report without synthesis*,
- Hajnsek, I. et al., 2009. *BioSAR 2008 Technical Assistance for the Development of Airborne SAR and Geophysical Measurements during the BioSAR 2008 Experiment*, Report. ESA Contract No: 22052/08/NL/CT. Oberpfaffenhofen, Germany, Linköping, Sweden, Toulouse, France, Milan, Italy: European Space Agency.

- Hallberg, B., 2007. *Synthetic-Aperture Radar Imaging of Forests in the VHF and UHF Bands: Electromagnetic Models and Data Analysis*. Chalmers Technical University.
- Hurtado, D.M., 2012. *Interferometric Processing of TanDEM-X Images for Forest Height Estimation*. Aalto University.
- Hyypä, J. et al., 2008. Review of methods of small-footprint airborne laser scanning for extracting forest inventory data in boreal forests. *International Journal of Remote Sensing*, 29(5), pp.1339–1366.
- Imhoff, M.L., 1995. Radar backscatter and biomass saturation: Ramifications for global biomass inventory. *Geoscience and Remote Sensing, IEEE Transactions on*, 33(2), pp.511–518.
- Isenburg, M., Lastools. Available at: <http://rapidlasso.com/lastools/>.
- Izzawati, Wallington, E.D. & Woodhouse, I.H., 2006. Forest Height Retrieval From Commercial. *IEEE Transactions on Geoscience and Remote Sensing*, 44(4), pp.863–870.
- Joanneum Research, Remote Sensing Graz. Available at: <http://dib.joanneum.at/rsg/>.
- Karjalainen, M. et al., 2012. Prediction of plot-level forest variables using TerraSAR-X stereo SAR data. *Remote Sensing of Environment*, 117, pp.338–347.
- Kaup, V.H. et al., 1983. Simulation of Spaceborne Stereo Radar Imagery: Experimental Results. *IEEE Transactions on Geoscience and Remote Sensing*, GE-21(3), pp.400–405.
- Knyazikhin, Y. et al., 1998. Estimation of vegetation canopy leaf area index and fraction of absorbed photosynthetically active radiation from atmosphere-corrected MISR data. *Journal of Geophysical Research*, 103(D24), pp.32239–32256.
- Kugler, F. et al., 2014. TanDEM-X Pol-InSAR performance for forest height estimation. *IEEE Transactions on Geoscience and Remote Sensing*, 52(10), pp.6404–6422.

- Kvålseth, T., 1985. Cautionary note about R 2. *The American Statistician*, 39(4), pp.279–285.
- Leberl, F., 1979. Accuracy analysis of stereo side looking radar. *Photogrammetric Engineering and Remote Sensing*, 45(8), pp.1083–1096.
- Lehner, M. & Müller, R., 2003. Quality check of MOMS-2P orthoimages of semi-arid landscapes. In *ISPRS Workshop High Resolution Mapping from Space*. 6-8 October 2003, Hannover, Germany.
- Li, F.K. & Goldstein, R.M., 1990. Studies of multibaseline spaceborne interferometric synthetic aperture radars. *IEEE Transactions on Geoscience and Remote Sensing*, 28(1), pp.88–97.
- Lohne, T.P., 2012. Radargrammetric Surface Models from RADARSAT-2 in Indonesia: Processing and Application in Tropical Forest Monitoring. , p.65.
- Lämås, T., 1996. *Forest management planning for biodiversity and timber production*. Swedish university of agricultural sciences.
- Makkonen, M. et al., 2012. Highly consistent effects of plant litter identity and functional traits on decomposition across a latitudinal gradient. *Ecology letters*, 15(9), pp.1033–41.
- Marklund, L.G., 1987. *Biomass functions for Norway spruce (Picea abies (L.) Karst.) in Sweden*, Umeå, Sweden: Swedish University of Agricultural Sciences.
- Marklund, L.G., 1988. *Biomassfunktioner för tall, gran och björk i Sverige*, Umeå, Sweden.
- Mercer, J.B., 1995. SAR Technologies for Topographic Mapping. In D. Fritsch & D. Hobbie, eds. *Photogrammetric Week "95."* 11-15 September 1995: Wichmann Verlag, Heidelberg, 1995, pp. 117–126.
- Mette, T., 2007. *Forest biomass estimation using polarimetric SAR interferometry*.
- Mette, T., Papathanassiou, K. & Hajnsek, I., 2004. Biomass estimation from polarimetric SAR interferometry over heterogeneous forest

- terrain. In *IEEE International Geoscience and Remote Sensing Symposium*. 20-24 Sep, 2004, Anchorage, Alaska: IEEE, pp. 511–514.
- Myneni, R.. et al., 2002. Global products of vegetation leaf area and fraction absorbed PAR from year one of MODIS data. *Remote Sensing of Environment*, 83(1-2), pp.214–231.
- Næsset, E., 1997a. Determination of mean tree height of forest stands using airborne laser scanner data. *ISPRS Journal of Photogrammetry and Remote Sensing*, 52(2), pp.49–56.
- Næsset, E., 1997b. Estimating Timber Volume of Forest Stands Using Airborne Laser Scanner Data. *Remote Sensing of Environment*, 61(2), pp.246–253.
- Næsset, E. et al., 2004. Laser scanning of forest resources: the nordic experience. *Scandinavian Journal of Forest Research*, 19(6), pp.482–499.
- Næsset, E., 2002. Predicting forest stand characteristics with airborne scanning laser using a practical two-stage procedure and field data. *Remote Sensing of Environment*, 80(1), pp.88–99.
- Neeff, T. et al., 2005. Tropical forest measurement by interferometric height modeling and P-band radar backscatter. *Forest Science*, 51(6), pp.585–594.
- Neumann, M. et al., 2012. Assessing Performance of L- and P-Band Polarimetric Interferometric SAR Data in Estimating Boreal Forest Above-Ground Biomass. *IEEE Transactions on Geoscience and Remote Sensing*, 50(3), pp.714–726.
- Nilsson, M., 1996. Estimation of tree heights and stand volume using an airborne lidar system. *Remote Sensing of Environment*, 56(1), pp.1–7.
- Näslund, M., 1947. *Funktioner och tabeller för kubering av stående träd*,
- Oliver, C. & Quegan, S., 2004. *Understanding synthetic aperture radar images*, United States of America: SciTECH Publishing Inc.

- Pan, Y. et al., 2011. A large and persistent carbon sink in the world's forests. *Science (New York, N.Y.)*, 333(6045), pp.988–993.
- Papathanassiou, K.P. & Cloude, S.R., 2001. Single-baseline polarimetric SAR interferometry. *IEEE Transactions on Geoscience and Remote Sensing*, 39(11), pp.2352–2363.
- Perko, R. et al., 2010a. Analysis of 3D Forest Canopy Height Models Resulting from Stereo-Radargrammetric Processing of TerraSAR-X Images. In *30th EARSeL symposium, Remote Sensing for Science, Education, and Natural and Cultural Heritage*. May 31 - June 3, 2010, UNESCO headquarters, Paris, France, p. 8.
- Perko, R. et al., 2011. Forest assessment using high resolution SAR data in X-band. *Remote Sensing*, pp.792–815.
- Perko, R. et al., 2010b. The capabilities of TerraSAR-X imagery for retrieval of forest parameters. In *ISPRC TC VII Symposium*. July 5-7, 2010, Vienna, Austria. Vol. XXXVIII, Part 7B, pp. 452–456.
- Persson, H. & Fransson, J.E.S., 2014. Forest Variable Estimation Using Radargrammetric Processing of TerraSAR-X Images in Boreal Forests. *Remote Sensing*, 6(3), pp.2084–2107.
- Petersson, H., 1999. *Biomassfunktioner för trädfaktorer av tall, gran och björk i Sverige*, Arbetsrapport 59, 1999, Sveriges Lantbruksuniversitet.
- La Prade, G., 1963. An analytical and experimental study of stereo for radar. *Photogrammetric Engineering*, 29(2), pp.294–300.
- Praks, J. et al., 2012. Boreal forest tree height estimation from interferometric TanDEM-X images. In *IEEE International Geoscience and Remote Sensing Symposium*. Munich, Germany, 22-27 July, 2012, pp. 1262–1265.
- Pulliainen, J.T. et al., 1994. Backscattering Properties of Boreal Forests at the. *IEEE Transactions on Geoscience and Remote Sensing*, 32(5), pp.1041–1050.
- Radio spectrum, 2014. Radio spectrum. *Wikipedia*. Available at: http://en.wikipedia.org/wiki/Radio_spectrum.

- Raggam, H. et al., 2008. Assessment of the potential of TerraSAR-X with respect to mapping applications using radargrammetric and interferometric techniques. In *Proceedings of the 3rd TerraSAR-X Workshop*. Nov 25-26 2008, Oberpfaffenhofen, Germany, p. 11.
- Raggam, H. et al., 2010. Assessment of the Stereo-Radargrammetric Mapping Potential of TerraSAR-X Multibeam Spotlight Data. *IEEE Transactions on Geoscience and Remote Sensing*, 48(2), pp.971–977.
- Raggam, H., Gutjahr, K. & Almer, A., 1997. MOMS-2P und RADARSAT: Neue Sensoren zur stereometrischen Geländemodellerstellung. *Vermessung & Geoinformation*, 4, pp.267–280.
- Raggam, H., Perko, R. & Gutjahr, K., 2009. Investigation of the stereo-radargrammetric mapping potential of TerraSAR-X. In *Proceedings of the 29th annual EARSeL Symposium*. Jun 15-18, 2009. Chania, Greece, pp. 371–380.
- Rawlings, J.O., Pantula, S.G. & Dickey, D.A., 1998. *Applied Regression Analysis: A Research Tool, Second Edition Springer Texts in Statistics* 2nd ed., New York: Springer.
- Reutebuch, S.E. et al., 2003. Accuracy of a high-resolution lidar terrain model under a conifer forest canopy. *Canadian Journal of Remote Sensing*, 29(5), pp.527–535.
- Richards, J.A., Sun, G. & Simonett, D.S., 1987. L-Band Forest Stands. *IEEE Transactions on Geoscience and Remote Sensing*, GE-25(4), pp.487–498.
- Rombach, M. & Moreira, J., 2003. Description and applications of the multipolarized dual band OrbiSAR-1 InSAR sensor. In *Proceedings of International Conference Radar*. 3-5 Sep 2003, Adelaide, Australia, pp. 245–250.
- Rosen, P.A. et al., 2000. Synthetic Aperture Radar Interferometry. In *Proceedings of the IEEE*. pp. 333–382.
- Rosenfield, G.H., 1968. Stereo Radar Techniques. *Photogrammetric Engineering*, 34, pp.586–594.

- Santoro, M., 2003. *Estimation of biophysical parameters in boreal forests from ERS and JERS SAR interferometry*. Friedrich-Schiller-University.
- Santoro, M. et al., 2002. Stem volume retrieval in boreal forests from ERS-1/2 interferometry. *Remote Sensing of Environment*, 81(1), pp.19–35.
- Schubert, A. et al., 2008. Geometric validation of TerraSAR-X high-resolution products. In *3rd TerraSAR-X Workshop*. November 25-26, 2008. Oberpfaffenhofen, Germany, p. 6.
- Sherwin, C.W., Calif., A.C.E.S. & Ruina, J.P. ; Rawcliffe, R.D., 1962. Some Early Developments in Synthetic Aperture Radar Systems. *Military Electronics, IRE Transactions*, MIL-6(2), pp.111–115.
- Skolnik, M., 2008. *Radar Handbook, Third Edition*, McGraw-Hill Education.
- Smith, G., 1998. *ERS InSAR coherence for remote sensing of boreal forests*, Institutionen för radio- och rymdvetenskap, Chalmers tekniska högskola,.
- Soja, M.J. & Ulander, L.M.H., 2013. Digital Canopy Model Estimation from TanDEM-X Interferometry Using High-resolution Lidar DEM. In *IEEE International Geoscience and Remote Sensing Symposium*. 21-26 July 2013, Melbourne, Australia, pp. 165–168.
- Solberg, S. et al., 2010. Estimating spruce and pine biomass with interferometric X-band SAR. *Remote Sensing of Environment*, 114(10), pp.2353–2360.
- Solberg, S. et al., 2013. Monitoring spruce volume and biomass with InSAR data from TanDEM-X. *Remote Sensing of Environment*, 139, pp.60–67.
- Solberg, S., Riegler, G. & Nonin, P., 2015. Estimating Forest Biomass From TerraSAR-X Stripmap Radargrammetry. *IEEE Transactions on Geoscience and Remote Sensing*, 53(1), pp.154–161.
- Stocker, T.F. et al., 2013. *Climate Change 2013: The Physical Science Basis. Contribution of Working Group I to the Fifth Assessment Report of the Intergovernmental Panel on Climate Change*, IPCC.

- St-Onge, B., Hu, Y. & Vega, C., 2008. Mapping the height and above-ground biomass of a mixed forest using lidar and stereo Ikonos images. *International Journal of Remote Sensing*, 29(5), pp.1277–1294.
- Swedish National Forest Inventory, 2013. *Skogsdata 2013*, Umeå, Sweden.
- Sylvander, S., Cousson, D. & Gigord, P., 1997. Etude des performances géométriques des images RADARSAT. *Bulletin - Société française de photogrammétrie et de télédétection*, (148), pp.57–67.
- Söderberg, U., 1986. *Funktioner för skogliga produktionsprognoser: tillväxt och formhöjd för enskilda träd av inhemska trädslag i Sverige*, Umeå, Sweden: Sveriges lantbruksuniversitet.
- Toutin, T., 2000. Elevation Modeling from Satellite Data. In *Encyclopædia of Analytical Chemistry*. R.A. Meyers (Ed.), John Wiley & Sons Ltd., Chichester, UK, Vol. 10, pp. 8543–8572.
- Toutin, T., 1999. Error tracking of radargrammetric DEM from RADARSAT images. *IEEE Transactions on Geoscience and Remote Sensing*, 37(5), pp.2227–2238.
- Toutin, T., 2002. Impact of terrain slope and aspects on radargrammetric DEM accuracy. *ISPRS journal of photogrammetry and remote sensing*, 57(3), pp.228–240.
- Toutin, T., 1996. Opposite side ERS-1 SAR stereo mapping over rolling topography. *Geoscience and Remote Sensing, IEEE Transactions on*, 34(2), pp.543–549.
- Toutin, T. & Amaral, S., 2000. Stereo RADARSAT data for canopy height in Brazilian forests. *Canadian Journal of Remote Sensing*, 26(3), pp.189–199.
- Toutin, T. & Gray, L., 2000. State-of-the-art of elevation extraction from satellite SAR data. *ISPRS Journal of Photogrammetry and Remote Sensing*, 55(1), pp.13–33.
- Treuhaft, R.N., 2002. Forest leaf area density profiles from the quantitative fusion of radar and hyperspectral data. *Journal of Geophysical Research*, 107(D21), p.4568.

- Treuhaft, R.N. et al., 1996. Vegetation characteristics and underlying topography from interferometric radar. *Radio Science*, 31(6), pp.1449–1485.
- Treuhaft, R.N. & Siqueira, P.R., 2004. The calculated performance of forest structure and biomass estimates from interferometric radar. *Waves in Random Media*, 14(2), pp.S345–S358.
- Treuhaft, R.N. & Siqueira, P.R., 2000. Vertical structure of vegetated land surfaces from interferometric and polarimetric radar. *Radio Science*, 35(1), pp.141–177.
- Ulaby, F.T. & Elachi, C., 1990. *Radar Polarimetry for Geoscience Applications*, Artech House.
- Ulaby, F.T., Moore, R.K. & Fung, A.K., 1982. *Microwave Remote Sensing: Active and Passive, Vol. II - Radar Remote Sensing and Surface Scattering and Emission Theory*, Addison-Wesley Publishing Company, Advanced Book Program/World Science Division.
- Ulander, L.M.H. et al., 2010. *BioSAR 2010. Technical assistance for the development of airborne SAR and geophysical measurements during the BioSAR 2010 experiment: Final report*, ESA contract no. 4000102285/10/NL/JA/ef, Linköping, Sweden, Salon Air Cedex, France, Göteborg, Sweden, Umeå, Sweden.
- Ulander, L.M.H. et al., 2013. Effects of Tree Species and Season on Boreal Forest Biomass Estimates from TanDEM-X. In *TanDEM-X Science Meeting*. Oberpfaffenhofen, Germany.
- Ulander, L.M.H. & Hagberg, J.O., 1995. *Radiometric and Interferometric Calibration of ENVISAT-1 ASAR. Research Report No. 172*, Göteborg, Sweden: Chalmers tekniska högskola.
- United Nations, 1998. *KYOTO Protocol to the United Nations framework convention on climate change*,
- Wallerman, J. et al., 2010. Forest mapping using 3D data from SPOT-5 HRS and Z/I DMC. In *IEEE International Geoscience and Remote Sensing Symposium (IGARSS)*. 25-30 July, 2010, Honolulu, HI, USA, pp. 64–67.

- Wardle, D. a et al., 2003. Long-term effects of wildfire on ecosystem properties across an island area gradient. *Science (New York, N.Y.)*, 300(5621), pp.972–5.
- Vastaranta, M., Niemi, M., et al., 2014. Prediction of Forest Stand Attributes Using TerraSAR-X Stereo Imagery. *Remote Sensing*, 6(4), pp.3227–3246.
- Vastaranta, M. et al., 2012. SAR Radargrammetry and Scanning LiDAR in Predicting Forest Canopy. In *IGARSS 2012*. Munich, Germany, pp. 6515–6518.
- Vastaranta, M., Holopainen, M. & Karjalainen, M., 2014. TerraSAR-X Stereo Radargrammetry and Airborne Scanning LiDAR Height Metrics in Imputation of Forest Aboveground Biomass and Stem Volume. *IEEE Transactions on Geoscience and Remote Sensing*, 52(2), pp.1197–1204.
- Watson, R.T. et al., 2000. *IPCC Special Report: Land Use , Land-Use Change , and Forestry*, Cambridge University Press.
- Wegmuller, U. & Werner, C., 1997. Retrieval of vegetation parameters with SAR interferometry. *IEEE Transactions on Geoscience and Remote Sensing*, 35(1), pp.18–24.
- Wegmuller, U. & Werner, C.L., 1995. SAR interferometric signatures of forest. *IEEE Transactions on Geoscience and Remote Sensing*, 33(5), pp.1153–1161.
- Weisberg, S., 1985. *Applied Linear Regression, 2nd edition*, John Wiley & Sons, New York.
- Wermuth, M. et al., 2009. TerraSAR-X rapid and precis orbit determination. In *21st International Symposium on Space Flight Dynamics*. 28 Sep - 2 Oct, 2009, Toulouse, France, p. 13.
- Wheeler, K. & Hensley, S., 2000. The GeoSAR airborne mapping system. In *IEEE Radar Conference*. 7-12 May, Alexandria, USA, pp. 831–835.

- Wikström, P. et al., 2011. The Heureka forestry decision support system: an overview. *Mathematical and Computational Forestry & Natural-Resource Sciences*, 3(2), pp.87–94.
- Wiley, C.A., 1965. Pulsed doppler radar methods and apparatus. , p.15.
Available at: <http://www.google.com/patents/US3196436>.
- Wiley, C.A., 1985. Synthetic Aperture Radars. *Aerospace and Electronic Systems, IEEE Transactions on*, AES-21(3), pp.440–443.
- Woodhouse, I.H., 2006. Predicting backscatter-biomass and height-biomass trends using a macroecology model. *IEEE Transactions on Geoscience and Remote Sensing*, 44(4), pp.871–877.
- World Meteorological Organization, 2014. *Summary Report of the Sixteenth Session of the GCOS / GTOS / WCRP Terrestrial Observation Panel for Climate (TOPC-XVI)*, Ispra, Italy: World Climate Research Programme.

Acknowledgments

It just started, and I can already glimpse the end of my PhD just ahead of me. It feels like yesterday, but this time already contained so much. After spending several years abroad, I thought about returning to Sweden and I asked my lifelong friend Mattias Nyström to give me a tip, whenever a job or suitable PhD position was about to come up. About half a year later, he got back to me and I applied for the PhD position. I did not get it, instead the wild card and nowadays working colleague Mona Forsman got it. Instead another research fund had just been accepted to SLU so a second PhD position was advertised and this time, I got the position.

At the time when I started, our section “lived” in barracks, as the ordinary university building was rebuilt. I shared a room with Mattias, as we have known each other since we were children and he helped me out a lot in the beginning, getting into the SLU culture and administrative stuff and knocked on each and every door at the department, to personally present me. Our institution had about 140 employees, so it was quite an exercise. Mattias was already and has continued to be my probably most important friend. Thank you Mattias!

During this time at SLU, I have got to know lots of interesting people and good friends but without having the main task working out, it would be for nothing. Therefore, first and foremost, I would like to thank my main supervisor Dr. Johan “Frasse” Fransson, who seems to possess at least 48 hour per day. He handles so many tasks and always manages to keep up a cheerful mood, positive comments and good feedback! My first assistant supervisor Håkan Olsson has also played an important role by providing valuable discussions both in- as well as out-of-topic and for intelligent comments and reliable and honest reflections on my written manuscripts. He was also great and entertaining company when I went out in field to collect field data for a study that has not been presented in this thesis.

Many thanks to assistant supervisor Jörgen Wallerman for helping out with field data and statistical speculations. Assistant supervisors Lars Ulander and Leif Eriksson are thanked for technical support and answering questions and also for being good company at conferences. I would also like to thank my last assistant supervisor Maurizio Santoro and Gamma Remote Sensing AG for making my research visit of one semester in 2013 situated in Berne, Switzerland, possible.

My co-author and good colleague Maciej Soja has been very valuable during my PhD. He has offered me room for discussions at my level, without judging stupid questions or thoughts. He has offered inspiring ideas and dreams and he has very honestly and constructively commented on my work, in order to improve it. Professor Emeritus at Chalmers, Jan Askne, is thanked for fruitful discussions and inspiring presentations.

The co-workers at SLU are my closest colleagues and each and every one deserves a special thanks! They have always been willing to help, and I really appreciate the valuable discussions and help from Karin, Mattias, Peder, Johan H, Jonas B, and Jörgen. Special thanks also to Heather, who now leads the section and brings true love and really cares about also the inside of people. She has also reviewed this thesis. I want to thank Eva, Mats N, Jonas J, Ann-Helen, Kenneth, Mats H, Emma, Mona, Håkan, Nils and Mikael E, as well as my former colleagues Andreas P and Alessandro M, from the Section of Remote Sensing. I want to thank Anne-Maj, Ylva, Linda, Carina, Nanna and Pär for their administrative support and helping out with traveling specifications. I have also got valuable technical support from Hannes Raggam at Joanneum Research in Graz, Austria, as well as statistical and field support from Hans Petersson and Göran Ståhl at SLU.

During coffee breaks or by creating them, Per S, Carola, Martin V, Emanuel, Back Tomas and many more have delivered interesting dialogues, amusing discussions and great company. Thanks also go to my friends in the PhD council, where I was president 2012.

At Chalmers Erik Blomgren, Anders Berg and Jan Torgrimsson have helpfully helped out with radar questions and are therefore thanked.

Outside work, I spend a lot of time with different activities and would especially like to thank all of you for giving important perspective to life and for giving meaning outside work! Thanks to my dancing friends in Swingum. Thanks my friends from abroad, mostly coming from Switzerland and USA, where I have lived parts of my life. These include Barbara who moved to Sweden with me, Sarah, Pascal, Franz and Franziska. Thanks to Mia for being a great dance partner and thanks to Linda for your eagerness of dancing and learning more. Thanks to the

teachers at BA who continue correcting me and help me fulfil my dream of movement perfection.

My family means a lot to me, more than I dare to tell them. Thank you mum and dad for believing in me, supporting me and for critically asking challenging questions such as "Why? What then? What for?". Thanks for being there and welcoming me every time I visit home. Thank you Maggan. Thanks to my sister Lotta and her husband Fredrik for accepting me as I am, and their wonderful daughter Saga that has brought more fantastic light into my life. Thanks to my grandparents Emil and Ann-Britt for their infinite love and pleasure of always greeting me. I also think of my grandmother "Majken" that passed away during my PhD in the fall of 2013.

Now, time to move on. After all, this end is just another possibility of starting something new!